ABSTRACT

CONSTRUCTION AND USE OF AN ON-LINE MASS IDENTIFICATION SYSTEM

By

Michael David Edmiston

An on-line mass identification system, SIEGFRIED, has been built to aid in the study of nuclei far from β stability. SIEGFRIED is based on the time-of-flight method, and is used in conjunction with a He-jet transport system. SIEGFRIED can be used to label γ-ray energies or β-ray energies with the mass of the emitting nucleus. SIEGFRIED also has been used to help identify and measure the half-life of ^{47}Cr. There is evidence that another application may be measuring β-recoil energy distributions and β-ν angular correlations.

CONSTRUCTION AND USE OF AN ON-LINE MASS IDENTIFICATION SYSTEM

By

Michael David Edmiston

A DISSERTATION

Submitted to
Michigan State University
in partial fulfillment of the requirements
for the degree of

DOCTOR OF PHILOSOPHY

Department of Chemistry
Program in Chemical-Physics

1976

ACKNOWLEDGMENTS

Thanks to Bob Suter, LaVerne Schirch, and Richard Weaver for guiding me into a career of science. Not only are they excellent teachers, they also provide admirable examples of how to be a good human being.

Thanks to Bill McHarris and Ray Warner whose leadership and friendship made graduate school a pleasant experience in addition to an educational experience.

Special thanks to Ray Warner for the countless hours of assistance he offered during the construction, use, and understanding of SIEGFRIED.

Thanks to Ken Kosanke for his pioneering work with He-jets and his preliminary work on the SIEGFRIED system.

Thanks to Norval Mercer for the machining of the majority of SIEGFRIED's components. His design suggestions were most helpful, and his jokes and rib-poking were great fun.

Thanks to Alice Ridky for carefully typing this dissertation, and for her patience during the editing process.

Finally, thanks to my wife, Mary, and to my parents and family for their love and understanding.

TABLE OF CONTENTS

Appendix

LIST OF TABLES

LIST OF FIGURES

Figure

Figure

Page

LIST OF ABBREVIATIONS

In addition to standard IUPAP symbols, the following abbreviations appear in this dissertation:

Abbreviation	Definition
ADC	analog-to-digital converter
CEMA	Channel-Electron-Multiplier-Array
CFT	constant-fraction timing
DP	diffusion pump
ESPG	electrostatic particle guide
F	Fermi beta transition
G&D	gate and delay generator
Gnd	electrical ground
G-T	Gamow-Teller beta transition
HV	the high voltage accelerating potential in SIEGFRIED
LED	light emitting diode
LN_2	liquid nitrogen
NC	normally closed
NIM	nuclear instrument module
NO	normally open
Op-amp	operational amplifier
ORE	orthogonal recoil energy

Abbreviation	Definition
PDD	precision digital delay
PRE	parallel recoil energy
rf	radio frequency
SCA	single channel analyzer
TAC	time-to-amplitude converter
TFA	timing-filter amplifier
TGT	target-arget
TOF	time-of-flight
TRE	total recoil energy
TTL	transistor-transistor logic

1. INTRODUCTION

The study of short-lived nuclei has become popular because technical advances have made it possible and because theoretical justifications - many of which come about once the study has begun - are plentiful. Some of the underlying theoretical justifications and experimental difficulties will be mentioned in this dissertation, but the author suggests reference (Ma73) as a starting place for persons desiring more information.

The prime difficulties one finds when attempting to study short-lived nuclei are shortness of existence and lack of pure production. Advances in fast transport (e.g., the He-jet) have made shortness of existence a minor problem for nuclei as short-lived as about 10 msec. The problem of impurities is more difficult but can be solved by chemical separation if the half-lives are not too short ($t_{1/2}$ > several minutes). This can be pushed down to several seconds by doing fast chemistry with the He-jet (Ko74). There is also evidence that very fast separations can be performed via selective transport in a He-jet (Ko75). However, the fast chemical separations are rather messy and usually the separation is not complete. Clearly, a very fast, simple-to-use, and precise method of separating the desired activity from impurities would be a great asset. The method most appealing to many is on-line mass separation or isotope identification.

The thought of mass separation/identification traditionally brings to mind two procedures - the magnetic method and the time-of-flight (TOF) method. Several laboratories have opted for the magnetic method

because it can be very precise (with hopes of separating isobars) and magnetic systems seem conceptually simpler. However, an extremely difficult problem has arisen which is making life less than enjoyable for laboratories with magnetic systems. This problem deals with the interface between the target and the magnetic channel. Somehow the activity must be delivered to an ion source, ionized, and propelled through the magnet. This turns out to be far from trivial, and the ideal solution has not yet been found. In addition, these magnetic systems are very expensive. In view of these problems, the MSU group decided to look for other means of mass separation. An electric quadrupole filter was considered, but it also had ion source problems and had poor efficiency. What we considered to be a breakthrough occurred when the Texas A&M group demonstrated that recoils from α decay could be energy analyzed by TOF with their MAGGIE system (Ju71). They also suggested, and later showed (Ma74), that β recoils can be mass analyzed, and the MSU SIEGFRIED project was initiated toward this goal. These systems overcome the ion source problem because the ions are produced by the decay of the nucleus whose mass is being determined. The interface between the target and the machine is a He-jet system which both labs have developed into very reliable tools.

SIEGFRIED and MAGGIE have gone their own separate ways, mostly because of a difference in purpose behind them. MAGGIE was originally viewed as a means to measure masses very precisely (on the order of 1 part out of 10^7) with the intention of obtaining such things as β-decay Q-values. SIEGFRIED was viewed as a means to label β events (β or γ energies) with the mass as a tool for unravelling the nuclear

spectroscopy. However, the two systems are very similar in concept and it is fair to say that SIEGFRIED was patterned after MAGGIE.

2. SIEGFRIED DESIGN

As mentioned, the basic idea behind MAGGIE and SIEGFRIED is a time-of-flight measurement in which one of the timing signals is the radioactive decay of the nucleus whose mass is being measured. The sequence of events will now be given; refer to Figure 2-1.

Atoms which have recoiled from an in-beam target are brought to SIEGFRIED by a He-jet using a 0.8-mm by 9-m polyethylene capillary. The target recoils are sprayed through a skimmer (to remove most of the helium) and impinge on a plate called the "collecting surface" or just "collector". Presumably the target recoils are attached to some sort of large molecules, often called "clusters" by He-jet enthusiasts, and most of these cluster-recoil particles will stick to the collector.

When one of the target recoils undergoes β decay a number of events happen which are simultaneous in the time scale of interest. These events (β and ν emission, nuclear recoil, electron shake-off, γ and $\gamma^{\pm}$ emission) will be collectively referred to as a β event. If the β recoil was in the proper direction, the recoiling atom will often leave the collector. (The recoiling atom is generally an ion because of the electron shake-off associated with the β decay.) Since the collector is held at several kilovolts positive with respect to ground (HV), any positive ions will be accelerated down the flight path and any negative ions will be accelerated back to the collector. The positive ions which make it down the flight tube are detected by the Channel-Electron Multiplier-Array (CEMA). The difference in time

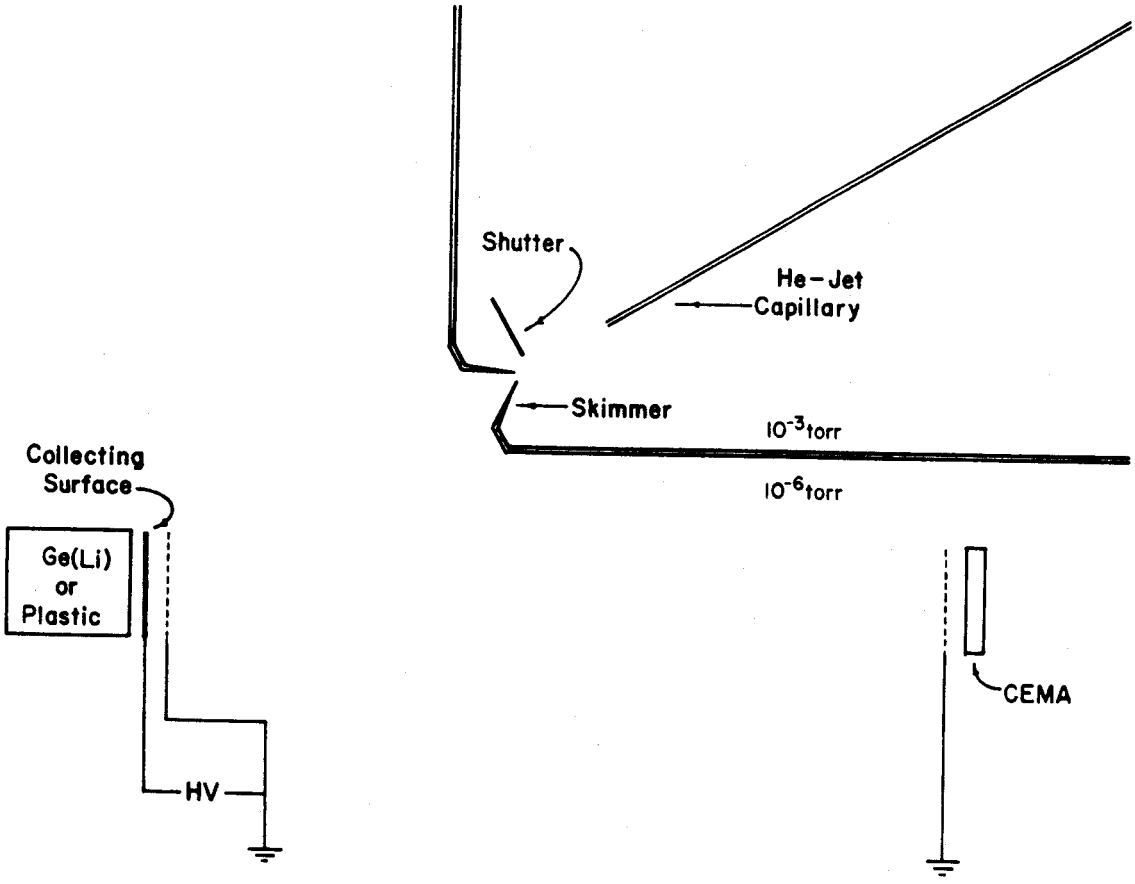

Figure 2-1. Schematic diagram of SIEGFRIED.

between detecting the β event and the CEMA event is the time-of-flight with which one can calculate the mass.

Since extremely precise mass measurements were not desired from SIEGFRIED, we designed SIEGFRIED to attain mass resolution of only 1 part out of 10^3. The major concern was to do anything which might improve the efficiency so that meaningful experiments could be performed in reasonable lengths of time. This difference of purpose between MAGGIE and SIEGFRIED lead to some differences in design, some of which were incorporated into the original design, and some added later. The *a priori* differences are a shorter flight path in SIEGFRIED, and a more normal angle between the He-jet and the collector. The shorter flight path should sacrifice resolution in favor of an efficiency increase for the CEMA detector. The larger angle should result in better efficiency of cluster-recoil collection. (Previous studies indicated that the more perpendicular the He-jet is to the collector, the more the cluster-recoils will tend to stick instead of bouncing off (Ko73).) MAGGIE's angle is 45 degrees whereas SIEGFRIED's is 60 degrees. Going from 45 to 60 degrees was not trivial in terms of design. It is not known whether the trouble was worth it, especially since it required a slight sacrifice in keeping the skimmer close to the collector.

One of the hardest choices that had to be made *a priori* was the choice of vacuum pump capacity. Most nuclei that had been studied prior to SIEGFRIED suggested that there was little loss in using a somewhat smaller capillary for the He-jet than usual. The usual capillary diameter is 1.4 mm with a helium flow of about 4000 ml/min (STP).

A 0.8-mm capillary seemed to give almost-as-good results with a helium flow of only 1000 ml/min (STP). There is much to be gained in terms of cost in choosing the smaller capillary because of the great expense of large vacuum equipment. The vacuum pumps are easily the greatest equipment cost of SIEGFRIED. Choosing to use the 0.8-mm capillary meant that we could use vacuum pumps that the lab already owned (we had to purchase only one pump out of seven). Recent results tend to indicate that nuclei with half-lives shorter than about one second cannot be easily studied with SIEGFRIED because of the choice of the small capillary. Whether the choice was good or bad is still not decided. Certainly had we chosen to use the larger capillary, the cost would have at least doubled. This capillary problem will be discussed again in a later section. A more detailed description of the vacuum system appears in Appendix A where one may also find directions on using the vacuum system.

Because SIEGFRIED has a large vacuum system, its physical size is impressive. Photographs of SIEGFRIED and of its various parts are shown in Appendix H.

3. ELECTRONICS

The electronics used to perform the mass measurement are standard NIM electronics common to most nuclear experimentalists. The β-event signal and the CEMA signal are suitably processed and sent to a time-to-amplitude converter (TAC). The output of the TAC is fed to an analog-to-digital converter (ADC); the output of the ADC is stored in a computer as a time-of-flight (TOF) spectrum. The energies of the β or γ rays can be similarly analyzed and recorded in coincidence with the mass (i.e., TOF). The β events are thus labeled with the mass of the nucleus from which they came.

It is easily seen then, that the electronics perform a simple delayed coincidence measurement. However, flight times are several microseconds, meaning that the delay must be several microseconds. This means that it is a little difficult to set the electronics so that all pulses appear at the computer at the correct time. The energy signal from the β event must be held or delayed for several microseconds until the TAC has an output ready. In order to preserve resolution it may be better to hold the signal and release it at the proper time rather than delay it with delay amps.

Another electronics point worth mentioning deals with the precision-digital-delay (PDD). Before building SEIGFRIED it was believed that the count rate in the β-event detector would be higher than that which can safely be used to start the TAC. To alleviate this problem it was decided to delay the β-event signal until after the CEMA signal and use the CEMA signal to start the TAC, using the delayed

β-event signal to stop the TAC. It would be good if the delay could be done with cables so that several β-event signals could be in the cable simultaneously. This would keep the dead time to a minimum. However, with delays of several microseconds, the cable would have to be very long and would require amplification and shaping along the length. It was therefore decided not to use cables, and the PDD was purchased. The PDD delays pulses from 0 to 100 μsec adjustable in steps of 1 nsec (reproducible and stable to 1 part in 10^5). It can handle count rates of up to the reciprocal of the delay or 10 MHz (whichever is less), and thus eliminates the problem if the β-event count rate gets too high. However, since it has its own dead time, the overall dead time of the system is comparable to the delay length.

It turns out that count rates seldom approach 10^4 counts per second, so the PDD is not really necessary. However, it has proven to be a valuable tool for several reasons. First, it provides an accurate and convenient means for calibrating the TAC. To calculate flight times the number of nsec per channel must be known for the TOF spectrum. The PDD can easily be set up to provide two or more TAC peaks which are separated by a well known time. Second, the PDD operates by counting a very stable 100-MHz oscillator. The output of the oscillator can be used to time other experiments which need a very accurate time base. Third, even though not required, the PDD is often used to delay the β-event signal so that the data can be collected in a spectrum of fewer channels. If the PDD is not used, the TAC-ramp period must be as long as the flight time. This means that to resolve adjacent mass peaks, the data must be collected in 4096 or 8192 channels.

Even then, the mass peaks get precariously close to each other for heavy masses. Also, some of the on-line analysis programs being written for the laboratory's PDP-11/45 computer would prefer a spectrum of fewer channels. This is easily done by running the TAC with a fast ramp, say 1 μsec, and then adjusting the PDD to put the masses of interest into the range of the TAC. For example, to measure masses in the region of mass 150, the flight times will be on the order of 10 μsec. Without the PDD the TAC would probably be run with a 20 μsec ramp period and the peaks would be about six channels apart if collected in a 4096-channel spectrum. However, if the PDD is used and the TAC has a ramp period of only 1 μsec, then adjacent masses will be 30 channels apart in a spectrum of only 1024 channels. Figure 3-1 shows three ways to make the mass measurement. Method 2 is slightly preferred unless the β-event count rate gets too high - then, method 3 would be preferred.

A detailed block diagram of the electronics will not be given in this section since SIEGFRIED requires some auxiliary electronics which have not yet been discussed. Detailed block diagrams will appear with the appropriate experiment, e.g., Figure 8-7.

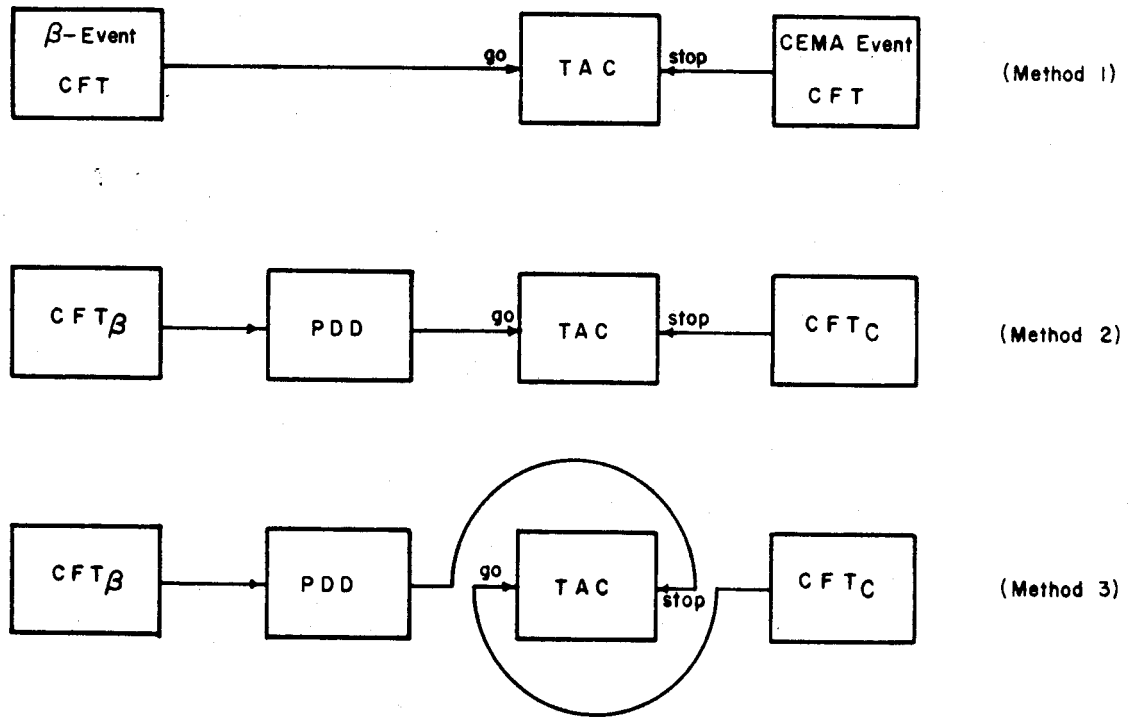

Figure 3-1. Three methods to perform the mass measurement.

4. INITIAL RESULTS

For testing purposes it has become standard to use an aluminum target and any of the available cyclotron beams. With most beams, one or more of the following nuclei can be made: ^{29}P, ^{30}P, ^{25}Si, ^{26}Si, ^{27}Si, ^{24}Al, ^{25}Al, ^{26}Al, ^{21}Mg, ^{22}Mg, ^{23}Mg, ^{20}Na, and ^{21}Na. All of these nuclides are ideal for study in SIEGFRIED because they have energetic decays to give good recoils, they have half-lives in a very good range for transport in the He-jet, and they represent a range of adjacent masses.

The result of an early attempt to use SIEGFRIED is shown in Figure 4-1. The beam was 76-MeV ^{3}He and the target was aluminum. Four peaks can be detected above background, and they are calculated to be masses 23, 26, 27, and 28. The prediction for this combination of beam and target is to make ^{23}Mg, ^{26}Si, ^{26}Al, ^{27}Si, and ^{28}Al. Thus the results make sense and it is obvious that SIEGFRIED works. It is also obvious that there are two big problems - the background is very high, and the peaks are too wide. An additional problem was that the count rates in the CEMA and Ge(Li) detectors seemed to be reversed. The CEMA had 5×10^{4} counts/sec and the Ge(Li) had 5×10^{3}. It was very difficult to believe that all the CEMA counts were from actual β recoils, so tests were performed to determine the properties of the CEMA counts.

The CEMA count rate is low if the cyclotron beam is off, even if there is appreciable radioactive material decaying on the collector. The CEMA rate rises very quickly when the beam is turned on and falls very quickly when the beam is turned off. The count rate can be

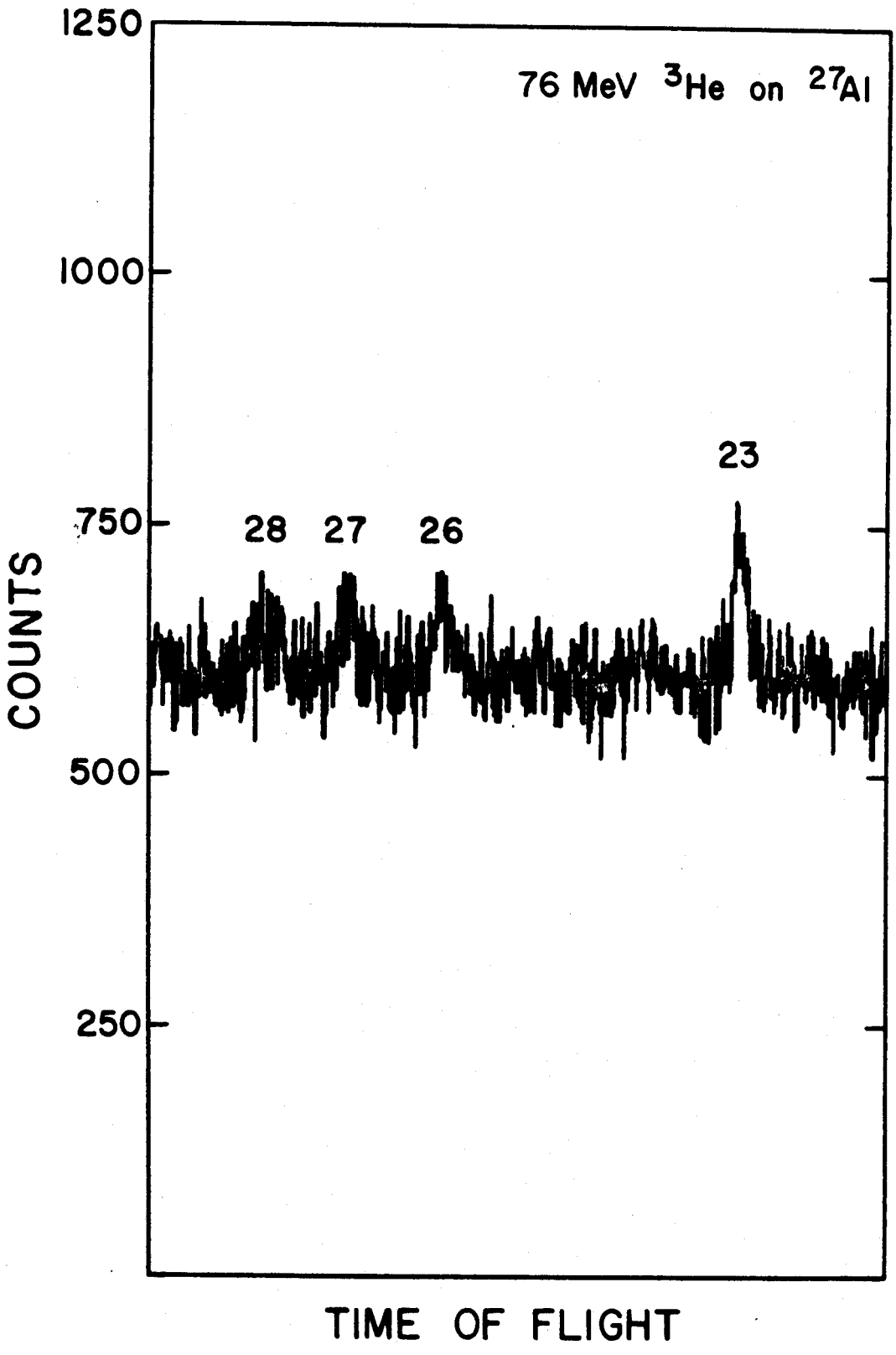

Figure 4-1. One of the first spectra obtained with SIEGFRIED.

dramatically changed by changing the level of the benzene impurity in the He-jet. Changing the polarity of the collector yields identical results. It is consistent with the data to say that as the cyclotron beam goes through the He-benzene mixture, it produces a plasma which is not relaxed by the time if reached SIEGFRIED. This plasma results in the spewing of both positive and negative ions into SIEGFRIED at a very high rate. The HV accelerates the positive plasma ions into the CEMA causing the high rate. The high CEMA rate causes many chance-coincidence events which give the high background.

Clearly, the high background is intolerable and something must be done to lower the CEMA rate. Since the rate depends on the benzene level, it was first thought that a different impurity at the proper concentration would yield good transport with less or a shorter-lived plasma. Many impurities were tried, but none were found which would yield a low CEMA rate, and none were found which would transport activity better than benzene.

5. THE SHUTTER

Although it is conceivable that the proper impurity at the proper concentration would yield both good transport and low plasma, the easiest solution is not to collect data and radioactivity at the same time. A mechanical shutter was constructed from a 12-volt relay. This was originally supposed to be a prototype, but it has worked so well that it is still in use. The relay flips a small piece of aluminum between the end of the capillary and the skimmer. The He-jet is thus completely cut off from the TOF chamber when the relay is actuated. When placed very close to the skimmer, the relay only has to move about 3 mm to go from a completely opened skimmer to a completely closed skimmer. Of course closure is not instantaneous, and even after closure it takes a few msec for the ions to clear out, but the shutter is fairly fast and has been operated at rates as high as 20 Hz.

A special NIM box was built which accepts a standard positive logic pulse to trigger the shutter. After a delay of from 0 to 1 sec, a positive logic pulse is emitted to gate data acquisition. The delay seems to work well when set to about 30 to 40 msec. This "shutter box" also contains a fairly linear ramp which starts at the same time the data pulse is emitted. The ramp can be used to time the interval between shutter closure and data events. The chance rate is so high when the shutter is open that if it ever fails to close during data acquisition, the accumulated data could be ruined. To safeguard against this, a phototransistor and light source are interlocked to the

shutter. If the light beam is broken by an unclosed shutter, the phototransistor output prohibits the logic pulse from enabling the ADC. This interlock is referred to as the "shutter failsafe".

The effects of the shutter are quite dramatic. Figure 5-1 shows a mass spectrum obtained when using the shutter with no delay, and Figure 5-2 shows the same spectrum when 30 msec of delay is inserted between the shutter pulse and the data-enable pulse. The shutter was set to be open for 14 sec and closed for 14 sec. The only difference between Figure 5-1 and Figure 5-2, other than the delay, is that Figure 5-2 shows data collected with a 38-MeV α beam instead of 36-MeV as in Figure 5-1. Notice the improvement in background because of the 30-msec delay. The chance-rate problem is eliminated, and the CEMA rate during data acquisition is a comfortable 50 to 100 counts per second.

Details of the shutter control box and operation can be found in Appendix C.

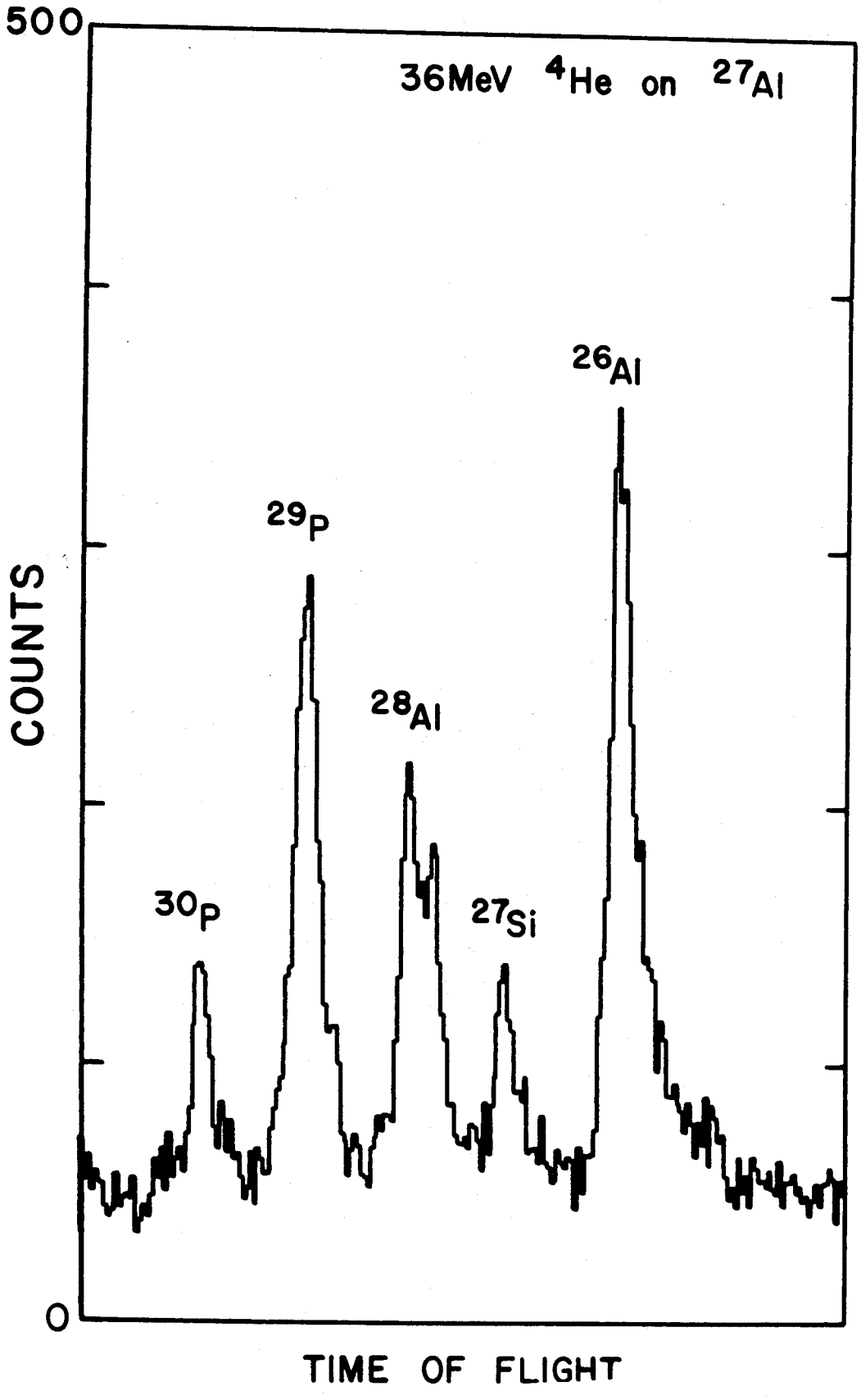

Figure 5-1. A shuttered spectrum without the delay.

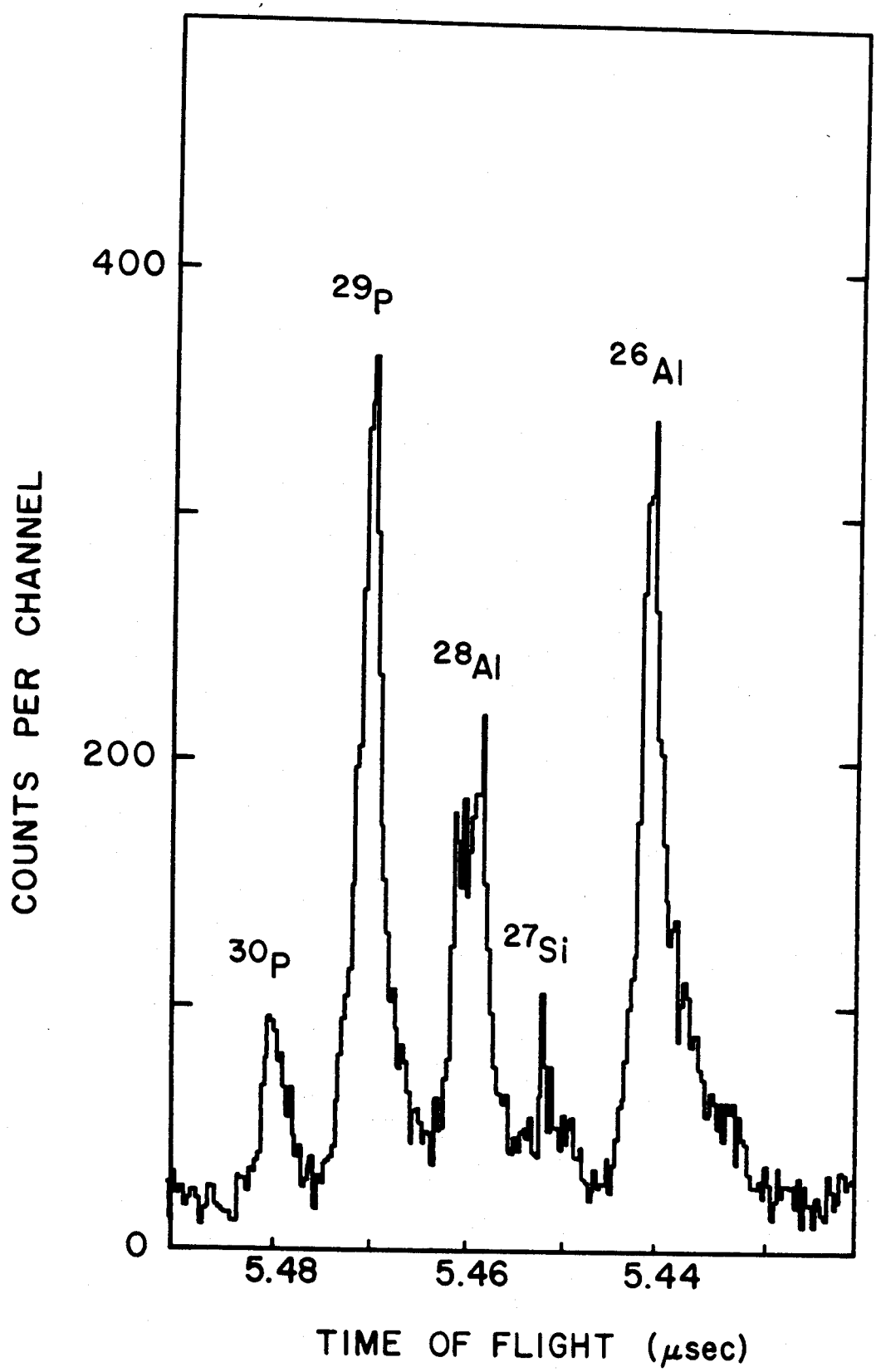

Figure 5-2. A shuttered spectrum with 30-msec delay.

6. RECOIL EFFECTS

The spectrum displayed in Figure 5-1 shows several phenomena which were quite unexpected. The peaks are all wider than the timing was known to be; they have strange tails on the low-mass side; they are slightly shifted (by varying amounts) toward lighter mass number; and the mass-28 peak is a doublet. It is now apparent that the cause of all this behavior is the uncertainty in the initial kinetic energy of the β recoil. This came as a surprise because it was not obvious to us that any of the recoils would be able to free themselves from the collecting surface without becoming almost completely thermalized. If the target recoils are really attached to some sort of large cluster molecule, then the β recoils should have a considerable barrier to penetrate. The method of attachment to the cluster molecules is not known, but it was thought that a plausible mechanism would be that the target recoil forms a seed on which the impurity ions condense. The target recoil would thus be buried on the collecting surface by perhaps several atomic layers of He-jet impurity residue. The β recoil has energy from about 0 eV to several hundred eV. It was hoped that the more energetic recoils might free themselves. In fact, the early MAGGIE system had an elaborate heated collecting surface to help the recoils leave it (Ma74). However, the SIEGFRIED evidence shows that not only do the β recoils free themselves, they also retain much of their original energy. This might be more consistent with a mechanism in which the recoil is attached to the surface of the cluster molecule.

The fast (ion-exchange) chemistry performed with the He-jet (Ko74) also leads to this conclusion, but again, very little is known about these interactions.

If we accept the fact that the recoils have a spread in energy of nearly their total possible kinetic energy, then the puzzling character of the spectrum shown in Figure 5-1 is readily explained. The peaks are wide because the kinetic energy spread shows up as a TOF spread. The peaks are slightly shifted because different nuclei have different β-decay Q-values and thus a different range of recoil energies. The strange shape is explained by considering geometry and kinematics. Refer to Figure 6-1.

When the ion recoils from the collecting surface, it has both an energy and a direction. The total energy is labeled TRE for total-recoil-energy. The energy can be broken down into a part that is parallel to the flight direction (PRE) and a part that is orthogonal to the flight direction (ORE). (Beware that energy is not a vector so it is velocity that defines the angle θ.) As the angle is increased for a given TRE (i.e., TRE constant, θ and ORE increase, PRE decreases), we reach a point where the trajectory misses the CEMA detector. The maximum value ORE can have and still yield a trajectory that hits the CEMA can easily be calculated and is found to be a very small number compared to the possible TRE values:

$$ORE_{max} = \frac{(\text{CEMA radius})^2}{(\text{Flight length})^2} \times (HV) \qquad (6\text{-}1)$$

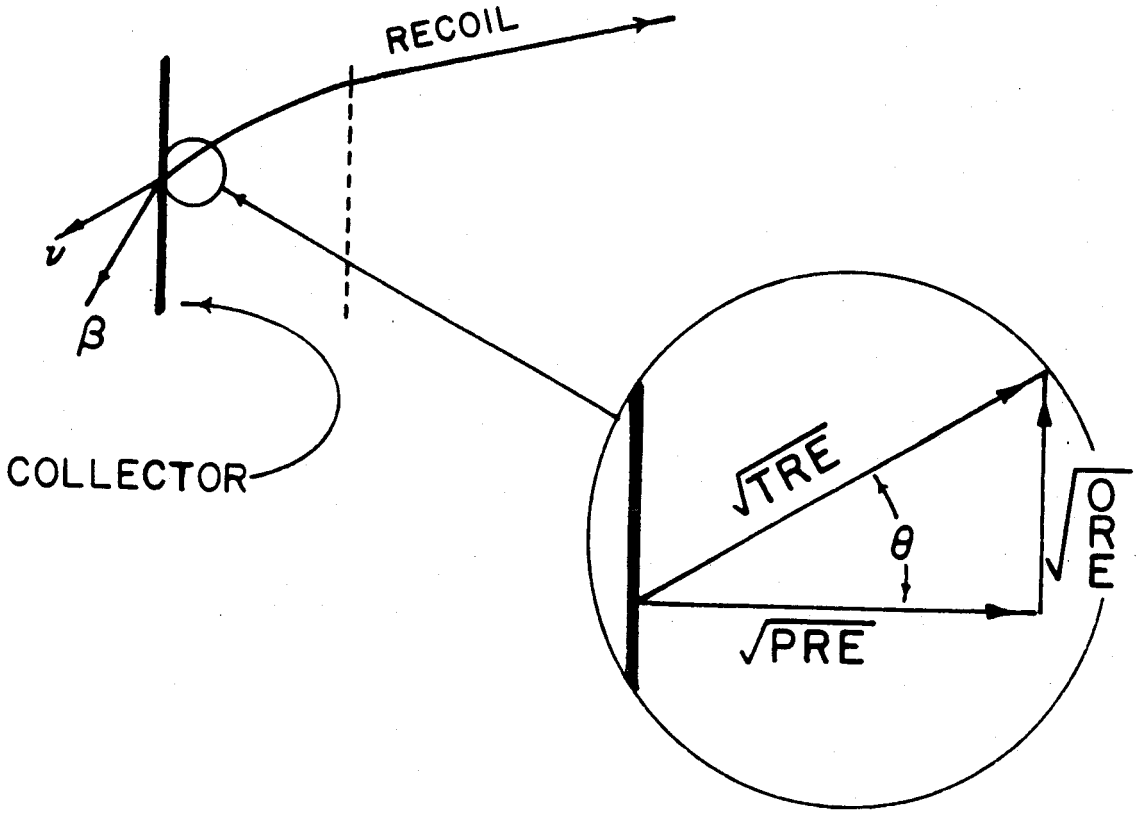

Figure 6-1. Definition of recoil components.

The spectrum shown in Figure 5-1 was taken with HV = 6 kV and a 110-cm flight path. The CEMA radius is 1.25 cm. Thus we have:

$$ORE_{max} = \frac{(1.25)^2}{(110)^2} \times 6000 = 0.77 \text{ eV} \qquad (6\text{-}2)$$

Since the recoils are coming off with tens and even hundreds of electron volts, it is obvious that the CEMA is not seeing most of the events. The ORE_{max} thus manifests itself as a strong bias against the more energetic recoils. This bias is what causes the peak shape to be reasonably narrow with a long tail on the low-mass side. We can see this more quantitatively by calculating the probabilities of seeing various recoil energies. Refer to Figure 6-2. For a given TRE, ORE_{max} defines a maximum angle, θ_m, calculated by the equation:

$$\theta_m = \arcsin\left(\frac{\sqrt{ORE_{max}}}{\sqrt{TRE}}\right) \qquad (6\text{-}3)$$

This angle defines a solid angle through which the recoil must pass if it is to be seen. The surface area contained in the solid angle is $2\pi(1 - \cos\theta)$. If the recoils are considered to be isotropic then the total area into which they could be emitted is 2π ($\frac{4\pi}{2}$, since they can only come off one side of the collector). Thus, the fraction of total recoils leaving the surface which are detectable with the CEMA is:

$$1 - \cos\left\{\arcsin\left(\frac{ORE_{max}}{TRE}\right)1/2\right\} \qquad (6\text{-}4)$$

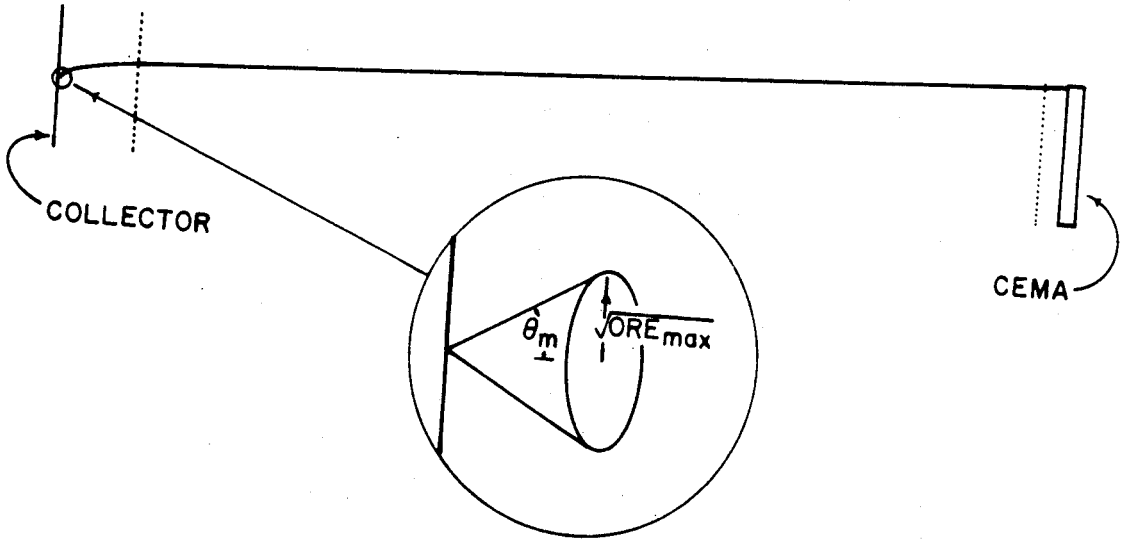

Figure 6-2. Definition of ORE_{max} and θ_m.

The trig functions can be eliminated giving:

$$\text{Fraction observable} = 1 - \left(\frac{\text{TRE} - \text{ORE}_{max}}{\text{TRE}}\right)^{1/2} \qquad (6\text{-}5)$$

A few values have been calculated for this function and appear in Table 6-1. ORE_{max} was set equal to 0.77 eV for the table.

Table 6-1

The Effects of ORE_{max}

TRE (eV)	Fraction Observable
1	0.52
5	0.08
10	0.039
50	0.0077
100	0.0039
500	0.0008

The selection against high energy recoils is readily apparent.

A recoil spectrum should appear something like Figure 6-3. (This is a very simple approximation; see Figure 11-1 for a more realistic spectrum.) If we multiply the values in Figure 6-3a by the equation for fraction observable, we get the distribution shown in Figure 6-3b. Note the similarity between Figure 6-3b and observed mass peaks.

Now is the time to explain the mass 28 splitting. The mass 28 peak results entirely from ^{28}Al, the decay of which is shown in Figure 6-4 (Le67).

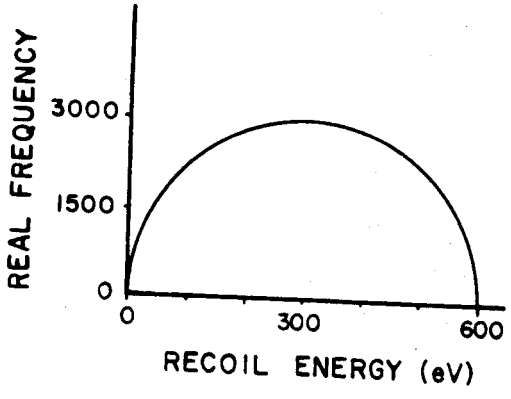

Figure 6-3a. An approximate β-recoil energy distribution.

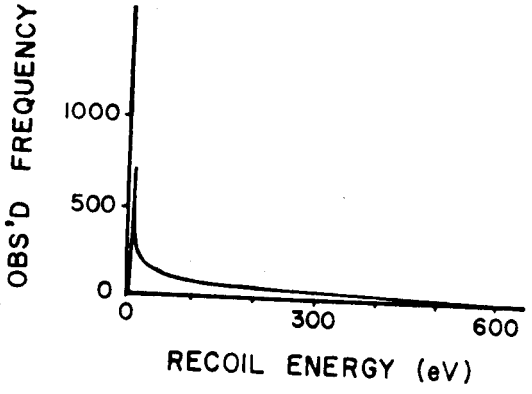

Figure 6-3b. The result of multiplying the curve in Figure 6-3a by the equation for the fraction of recoils observable.

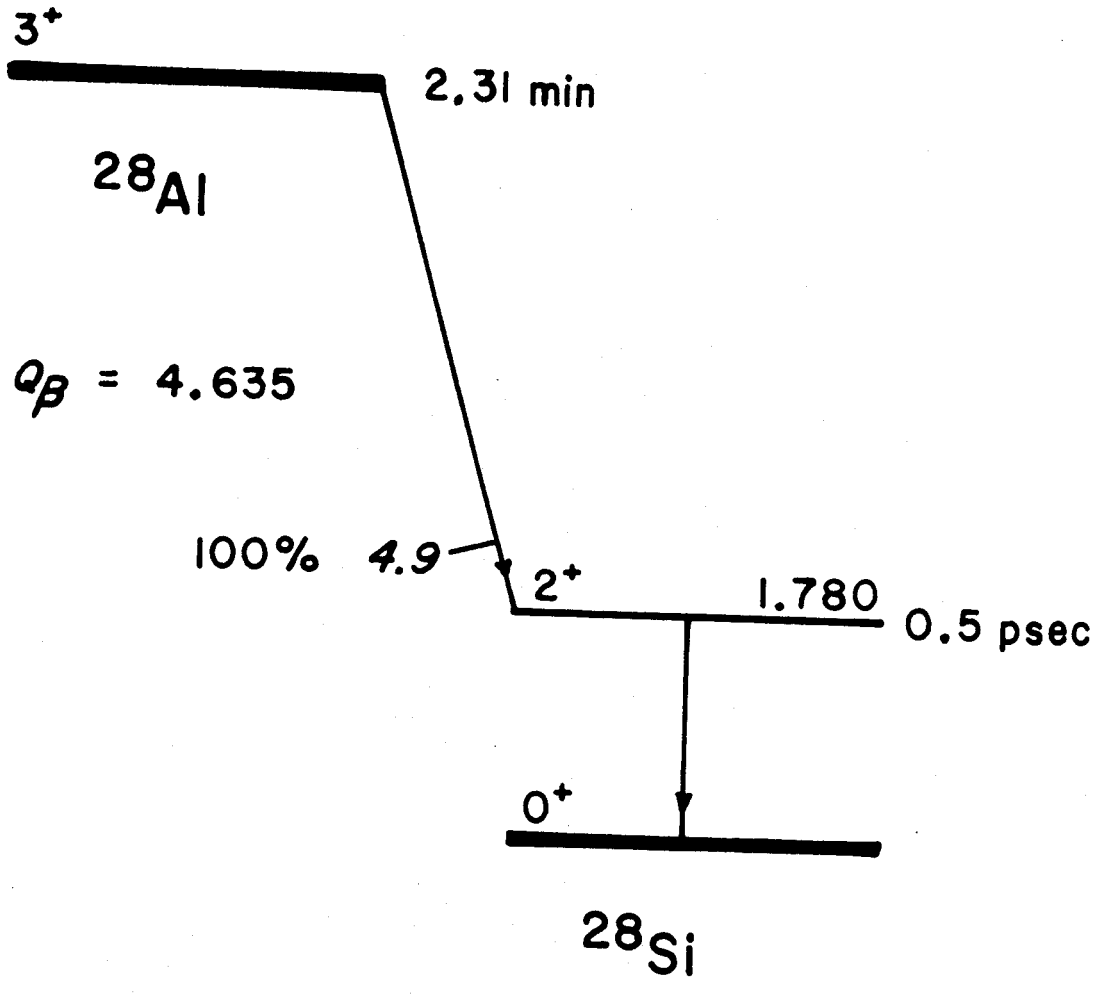

Figure 6-4. The decay of ^{28}Al.

There are two things about the ^{28}Al decay which are different from the decays of the other nuclides seen in Figure 5-1. First, ^{28}Al is a β^- decay, whereas the rest are β^+. Second, ^{28}Al always produces a 1.78-MeV γ ray, whereas the rest β decay only to ground states. The β^- aspect is important because SIEGFRIED's vacuum window and collector stop β rays with energy less than about 2 MeV. Thus, to detect ^{28}Al by the β^-, the β^- is constrained to have energy greater than 2 MeV. This is not true with the β^+ decays because if the β^+ is less than 2 MeV the decay can still be detected via the 511-keV $\gamma^{\pm}$. The 1.78-MeV γ ray is important because it can impart a recoil energy of 60 eV to the mass 28 atom. In describing the recoil, we see that there is a four body problem (β^-, $\bar{\nu}$, γ, ion). While the recoil from the γ is almost discrete, the recoil from the β^- and $\bar{\nu}$ are not; and furthermore, the observed β^- and $\bar{\nu}$ recoil distribution is perturbed (by the vacuum window) if the observation was made via the β^- rather than the γ. It makes intuitive sense, then, that there may be two peaks corresponding to whether the TAC was signaled by the β^- or the γ. It also makes sense that perhaps the splitting occurs merely because the geometry and very small ORE_{max} permit only certain combinations of the recoil components. Indeed, the splitting goes away (experimentally) when ORE_{max} is increased. Several models were calculated to try to reproduce the splitting. They all failed, probably because of too many simplifying assumptions. It was decided that a complete understanding of the splitting was not worth the effort it would take to do an exact calculation - if indeed an exact calculation can be done.

The phenomena seen in Figure 5-1 have now been explained. Unfortunately, the explanation also implies that SIEGFRIED is a very inefficient instrument since most of the recoils do not make it to the CEMA. We can see from equation (6-1) that if we raise the HV we also increase ORE_{max}. However, we are interested in much more dramatic results than we can obtain by raising the HV. (Even if we could raise the HV to 60 kV, we would only raise ORE_{max} to 8 eV. This is still small compared to the possible recoil energies.) In addition, raising the HV too high presents some new problems. First, the mass peaks will be compressed, meaning that to get adequate separation between adjacent masses we would have to increase the flight length. This would have the opposite effect on ORE_{max} than what we desire. There is also a problem in obtaining a high voltage supply that is stable enough for our purposes; and, there is a problem in avoiding sparks. Raising the HV alone is clearly not the best solution to the problem of a small ORE_{max}.

7. THE ELECTROSTATIC PARTICLE GUIDE

An improvement which gives the desired increase in ORE_{max} is the addition of an electrostatic particle guide (ESPG). The ESPG is simply a wire down the center of the flight tube to which a voltage is applied. As the name implies, the ESPG guides the particles from the collecting surface to the CEMA even if they have appreciable values of ORE. If the wire is perfectly straight, the field will be radial except for perturbations at the ends. The particles see almost no field in the flight direction and the TOF is unaffected. In the directions orthogonal to the flight, the particles see a field attracting them toward the wire. The diameter of the wire is very small, so the chances of the particles actually hitting it are slim, and they end up in an orbit about the wire. Since the particles have also been given a high velocity in the flight direction by the HV, the actual path is a helix with the ESPG as the axis. Figure 7-1 shows an "artist's conception" of a trajectory for an ion which would have missed the CEMA if the ESPG were not present.

The ESPG installed in SIEGFRIED is a 0.05-mm copper wire. In addition to presenting a very small cross-section for the particles to hit, the thinness of the wire also permits it to hang in a straight line with only moderate tension. The wire is supported on both ends by pieces of monofilament nylon fishing line. This helps to make the field perturbations at the ends a minimum. In addition, the power lead is attached at the CEMA end where its perturbation is only effective for a very short flight path. The actual design of the flight tube and

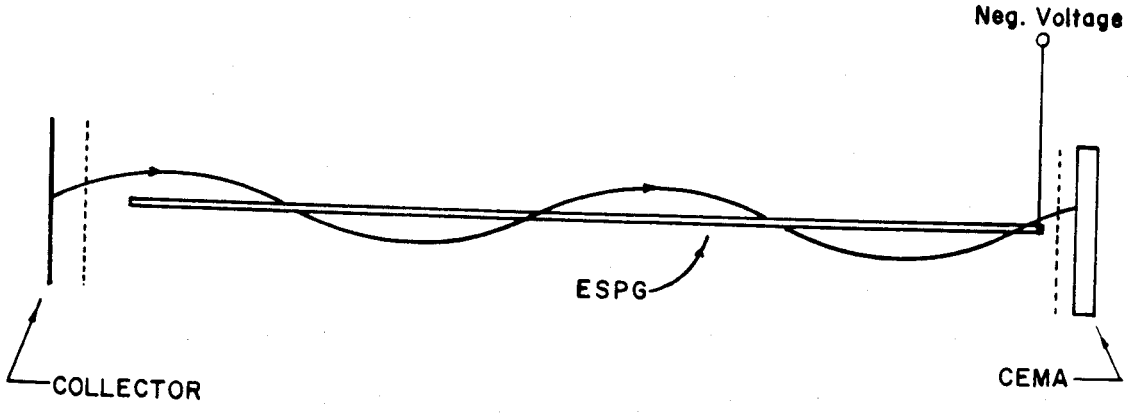

Figure 7-1. An "artist's conception" of an ion trajectory with the ESPG.

collector assembly prevents the ESPG from extending for the whole flight path. It starts about 7 cm from the first grid and ends 1 cm from the second grid. The distance at the beginning is unfortunate since it limits the ORE_{max}. With HV = 6 kV, ORE_{max} is about 40 eV because an ORE greater than this will cause the particle to hit the wall of the flight tube before it gets to the ESPG. However, 40 eV is a large improvement, and if the HV is now raised, it will have a large effect. For example, if HV = 18 kV, then ORE_{max} could be as high as 120 eV (if the ESPG voltage were high enough).

The results of the ESPG are perhaps even more dramatic than the results of the shutter. Figure 7-2 shows the results of a test in which each spectrum was collected under identical conditions for equal times with only the ESPG voltage varied. The spectra are thus a direct indication of the improvement in efficiency with the ESPG. It is comforting to note that the peak shapes do exactly what one would expect if the recoil phenomena explained earlier are correct. As the ORE_{max} is increased, the counts in the tails of the peaks increase since the discrimination against the higher-energy recoils is beginning to abate. The improved efficiency begins to change character at about 100 V, because by this point the ORE_{max} has become sufficiently large that all the recoils leaving the collecting surface with the correct PRE to place them in the first few channels are being seen. Once this occurs, the peaks begin to get wider faster than they get taller. The test was actually carried out to 2000 volts on the ESPG at which point the 25 to 29 mass peaks merged into one wide peak. Clearly the voltage on the ESPG must be chosen carefully to enable one to get the optimum

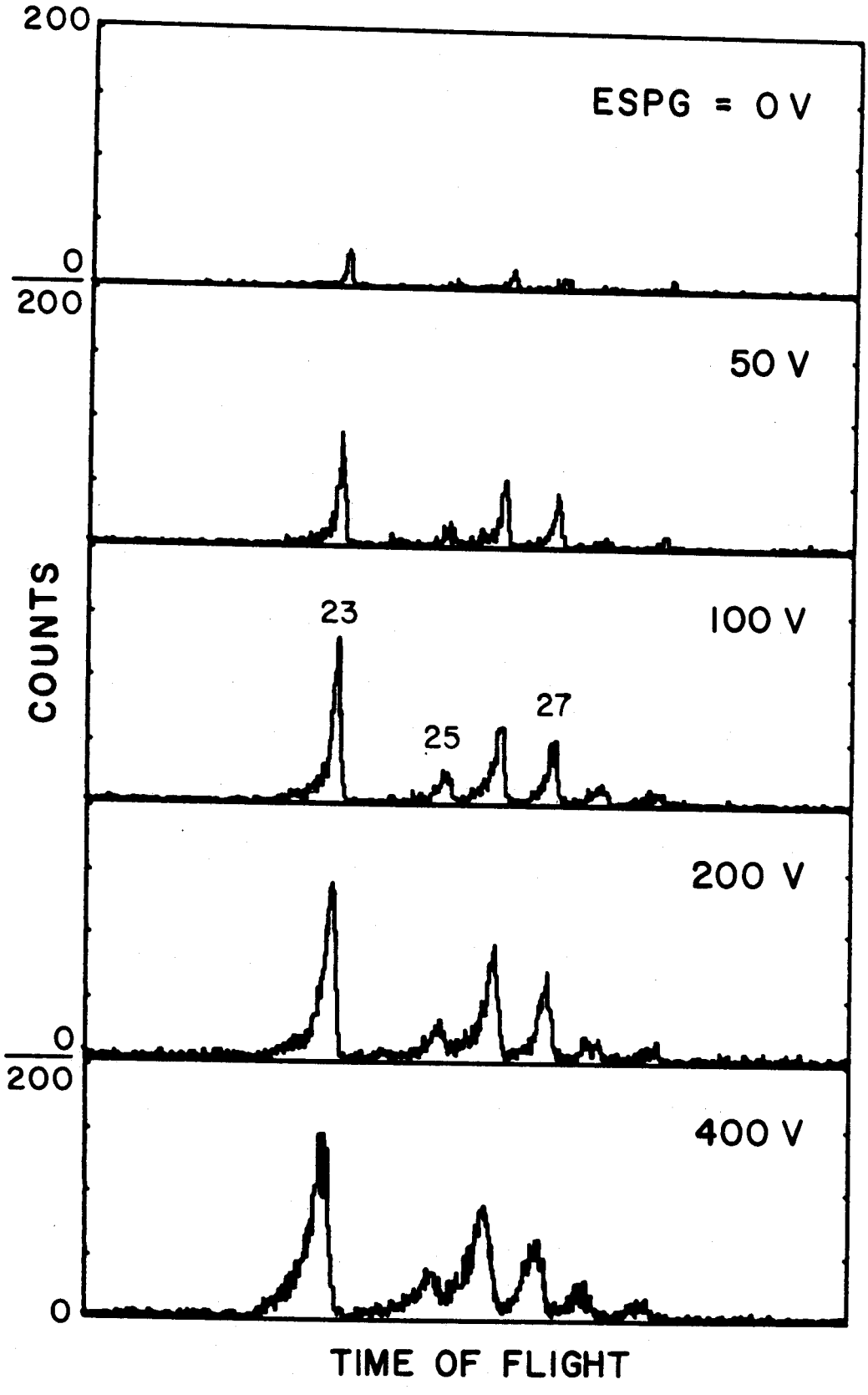

Figure 7-2. The effects of the ESPG at different voltages.

efficiency without losing too much resolution. It is at this point that an increase in HV can do wonders. The spread in the TOF can be calculated if the approximate spread in recoil energies are known:

$$\frac{\Delta TOF}{TOF} = \frac{-\Delta PRE}{2 \times HV} \qquad (7\text{-}1)$$

As mentioned in Section 6, there are two problems in raising the HV. First, the HV must be very stable and must not have much ripple. Second, the physical arrangement of the collecting surface and the detector ports makes it hard to go high in voltage without danger from sparks. (It is not desirable to add insulators between the collector and the β-event detector port because the insulator would stop low-energy β rays.) It was finally decided to purchase a 30-kV supply which is stable to 100 ppm/8 hr and has ripple less than 10 ppm. This was the highest voltage obtainable with such good stability, and is probably as high as one would want to go because sparking has already been a problem at 30 kV. In addition, 30 kV is about the highest voltage one would want to use without lengthening the flight path.

One disadvantage of the ESPG and a higher HV is the increased CEMA rate during activity collection. The ESPG and HV enhance the chances of seeing plasma ions just as well as they enhance seeing the β recoils. While this has no adverse effect on the data as long as the shutter is used, it greatly decreases the life of the CEMA. (According to the manufacturer, the CEMA life is proportional to the total amount of charge put through it.) Count rates with the shutter open get as high as 2×10^5 counts/sec, which is close to the maximum tolerable rate.

We can therefore expect the CEMA to last longer if we do something to reduce the rate during periods when the shutter is open. It will not work to turn the CEMA on and off because it can't be done quickly enough. (Not only does it take a little while for the CEMA bias supply to stabilize, it also is safer to increase and decrease CEMA voltage slowly.)

It was suspected that the ESPG could be used as a deflector by reversing its polarity when the shutter is open. This was tried and found to be true. A bipolar supply was built, and the ESPG now switches polarity in synchrony with the shutter. It is 110 volts negative during data acquisition and 270 volts positive during activity collection. The 110 volts seems to be about right when the HV is 6 kV. Perhaps the ESPG voltage could be raised when the HV is higher, but this was not attempted. For an example of how well SIEGFRIED works with the dual voltage ESPG and HV = 15 kV, please see Figure 7-3. Additional information concerning the 30-kV supply and the ESPG supply is given in Appendix E and Appendix F.

At this point it was decided that SIEGFRIED was ready to be put to use.

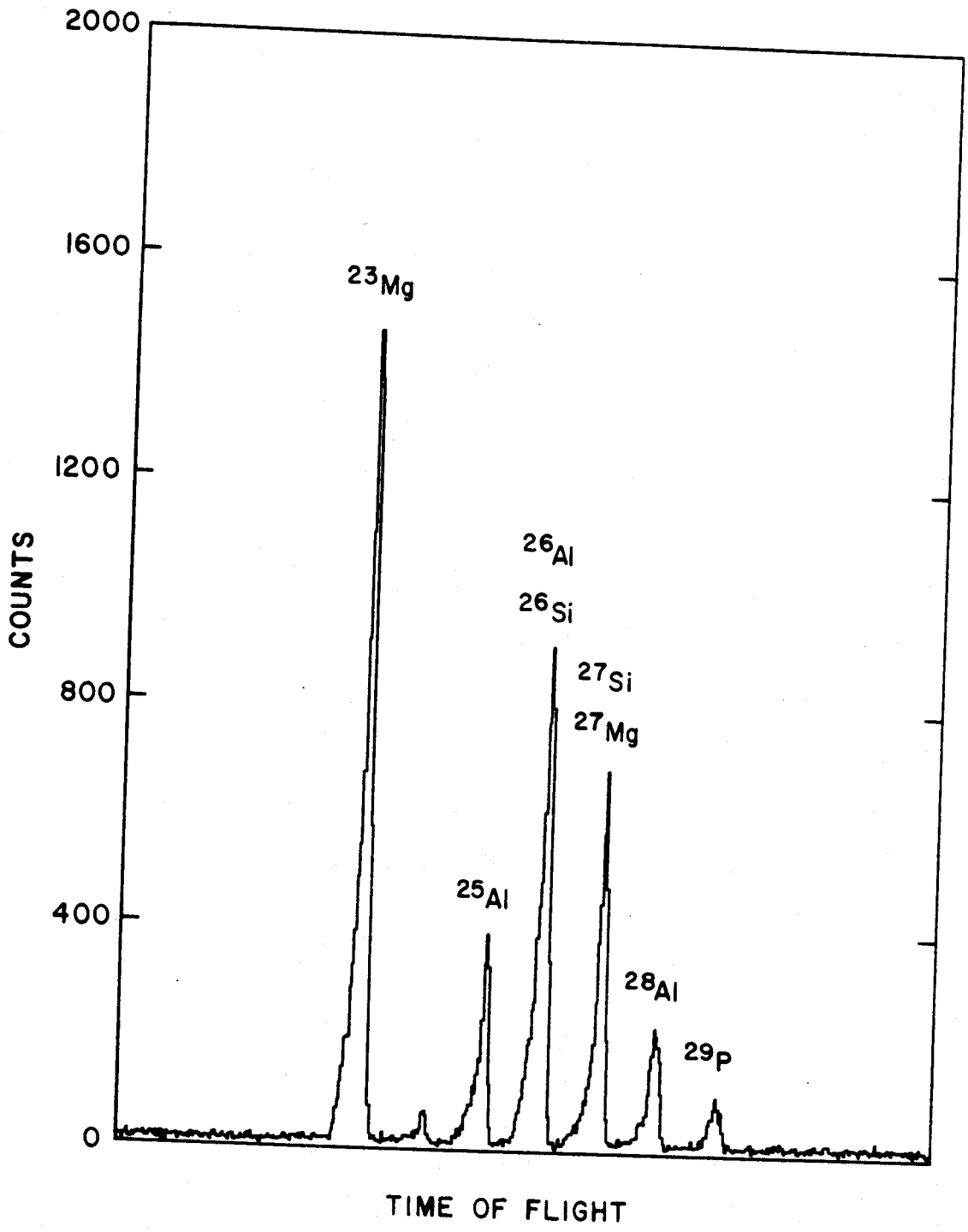

Figure 7-3. A typical spectrum from an aluminum target when SIEGFRIED is used in the usual manner. The beam was 70-MeV ^{3}He.

8. MIRROR β DECAYS

A mirror β decay is one in which the parent and daughter differ by having their proton numbers and neutron numbers reversed. Since the nuclear force is the same for both protons and neutrons, the parent and daughter should have very similar wave functions, differing only in the Coulomb displacement. This results in a large overlap between the initial and final states in the transition probability equation. It is possible to calculate the logft values from experimental data to check the agreement with those values which have been calculated theoretically. The experimental data needed are the masses of the parent and daughter (so the β-decay Q-value can be found) and the half-life of the parent. Until recently, the logft values were known for the proton-rich mirrors only for nuclei as heavy as ^{43}Ti. When the masses for the mirrors in the $f_{7/2}$ shell were measured very accurately at MSU (Mu74), interest was generated in measuring the half-lives for these nuclei. The half-lives are difficult to measure because they are short and also because many impurities are simultaneously produced. This is exactly the sort of problem that SIEGFRIED was built for. Measurements of these half-lives were thus chosen to be SIEGFRIED's first project.

The excitation functions for producing the mirrors were calculated using the ALICE code written by Blann and Plasil (Bl73). These functions fall into two groups depending upon whether the mirror has an odd number of protons or an odd number of neutrons. The odd-neutron group (^{47}Cr, ^{51}Fe, and ^{55}Ni) are produced by the (^{3}He,2n) reaction on targets of ^{46}Ti, ^{50}Cr, and ^{54}Fe. The ALICE results for these are shown in

Figures 8-1, 8-2, and 8-3. For these nuclei the proton is bound by only about 4 MeV. Thus, the (^{3}He,$p2n$) reaction begins to compete at only about 4 MeV above the Q-value for making the mirror nucleus of interest. The product of this competing reaction is in every case a very undesirable impurity. It has characteristics almost identical to the mirror in every way except for mass. For example, the impurity when trying to make ^{47}Cr is ^{46}V. ^{46}V has almost identical half-life to what one would expect for ^{47}Cr and also has a very similar β-decay Q-value. The α particle is also weakly bound, but this is not so much a problem in terms of impurities as it is in terms of lowering the cross-section for making the mirror nucleus of interest. The (^{3}He,α) product is long enough lived to be considered stable compared to the mirror. Notice that for these odd-neutron mirrors there is a region below the Q-value of the troublesome impurity in which the mirror can still be made.

The ALICE results for making the odd-proton mirrors are shown in Figures 8-4, 8-5, and 8-6 (only the mirror and the troublesome impurities are shown). In this case the α being loosely bound leads to the troublesome impurity. In the example of trying to make ^{45}V, we see that this leads to ^{42}Sc, which has characteristics very similar to the expected characteristics of ^{45}V. Here, however, when one runs at energy sufficiently low to avoid the (p,αn) reaction, the (p,n) reaction overlaps with the desired (p,$2n$) reaction. In the example of ^{45}V, this leads to the production of ^{46}V, which we have already seen is a problem.

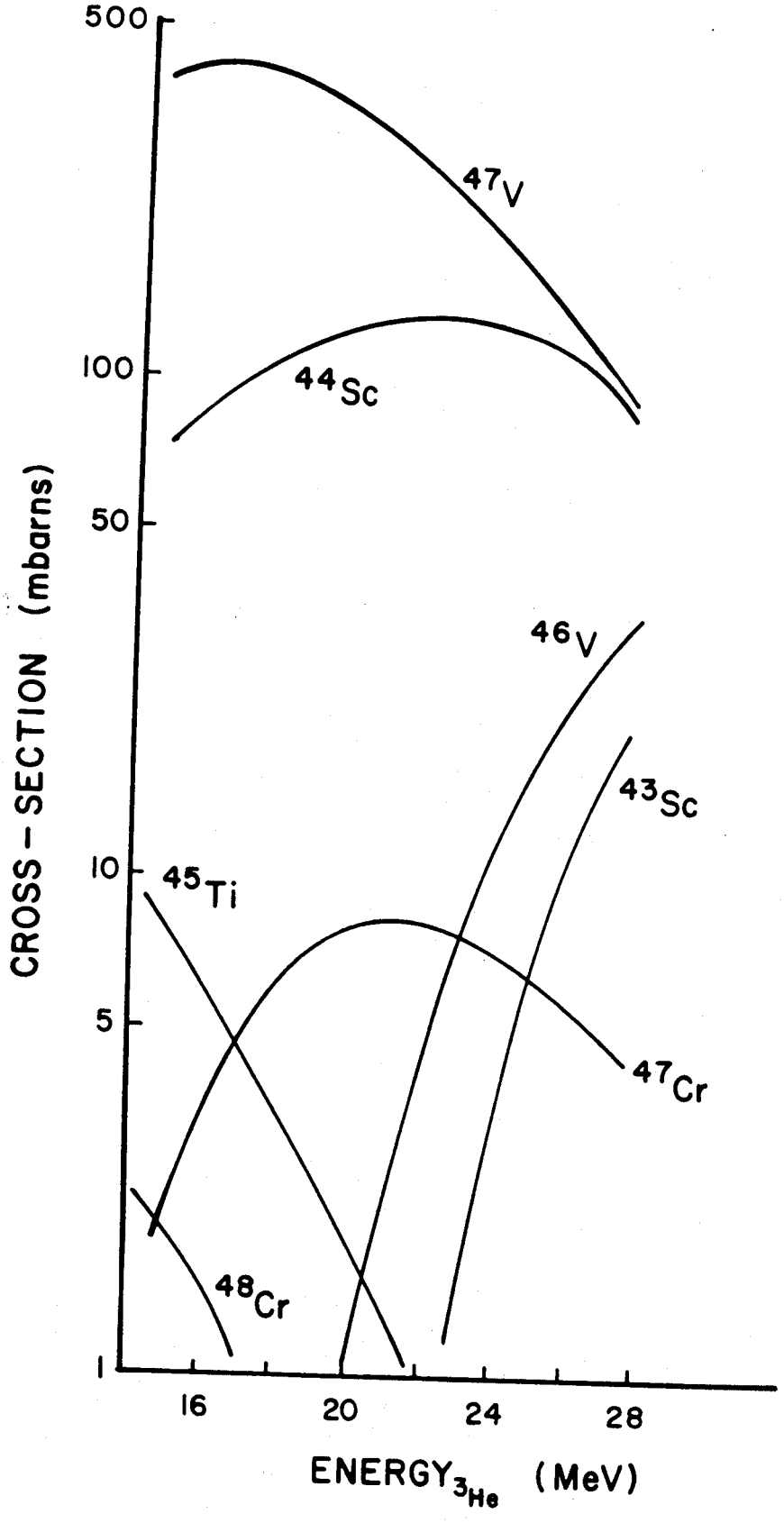

Figure 8-1. ALICE predictions for ^{3}He on ^{46}Ti.

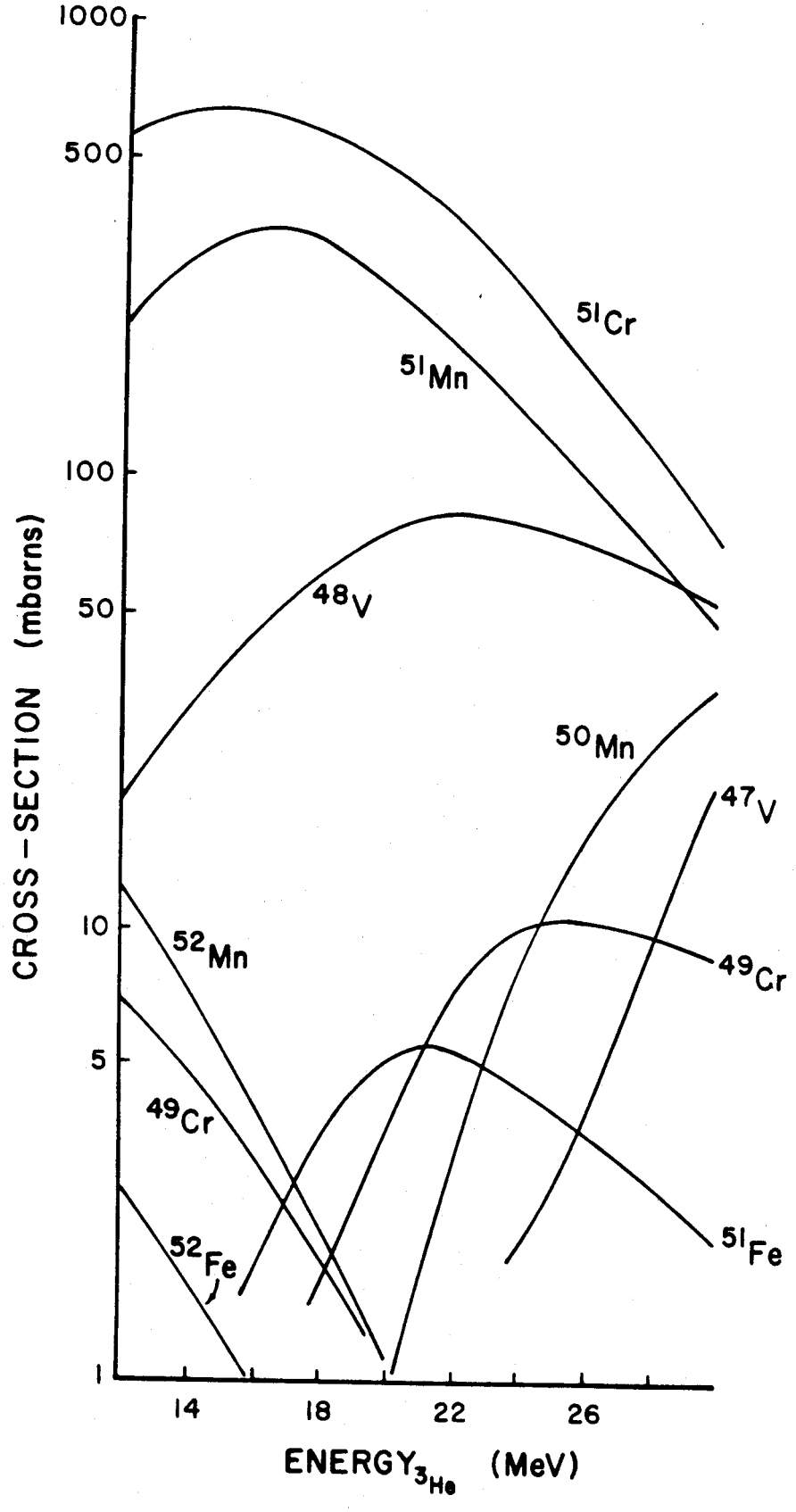

Figure 8-2. ALICE predictions for ^{3}He on ^{50}Cr.

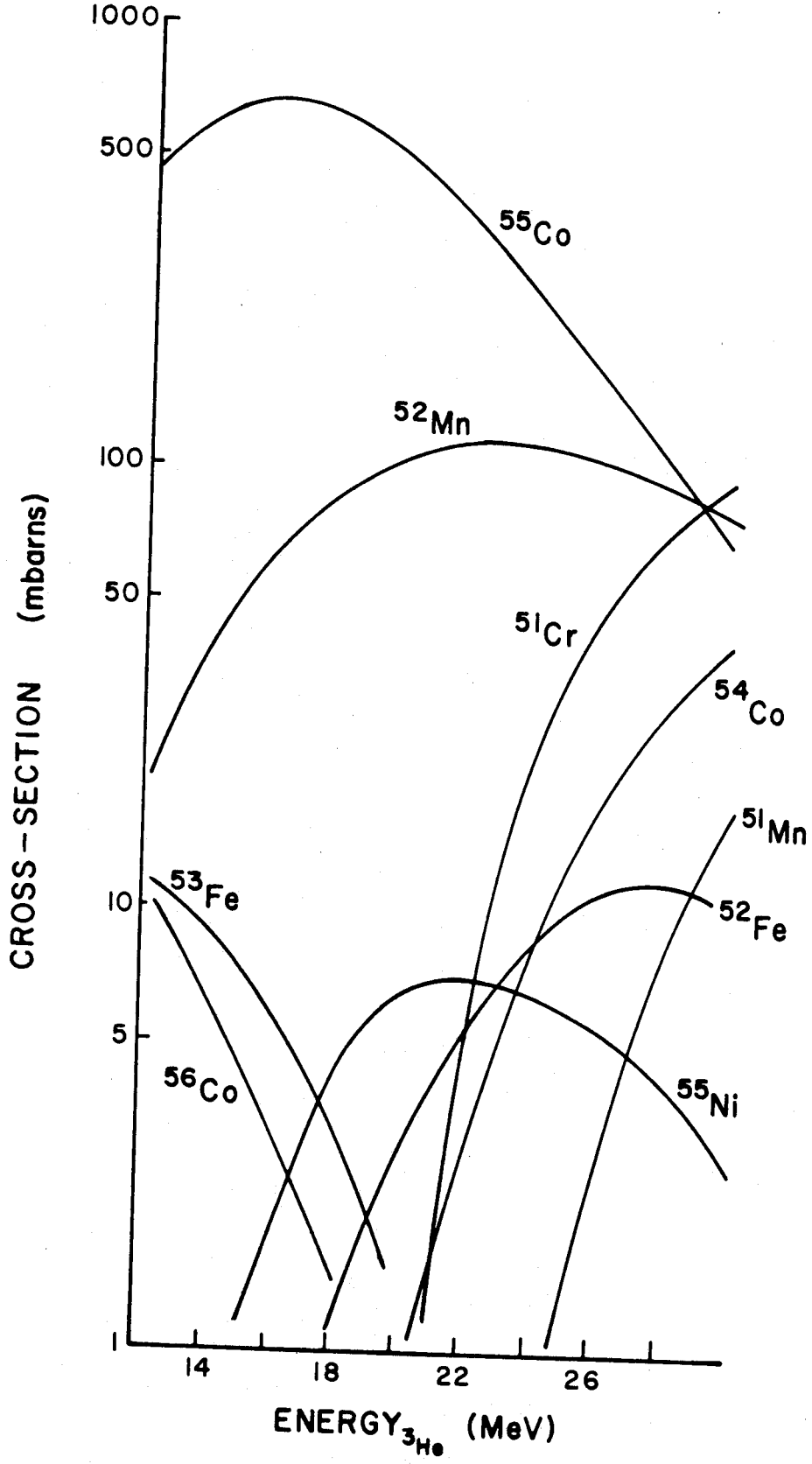

Figure 8-3. ALICE predictions for ^{3}He on ^{54}Fe.

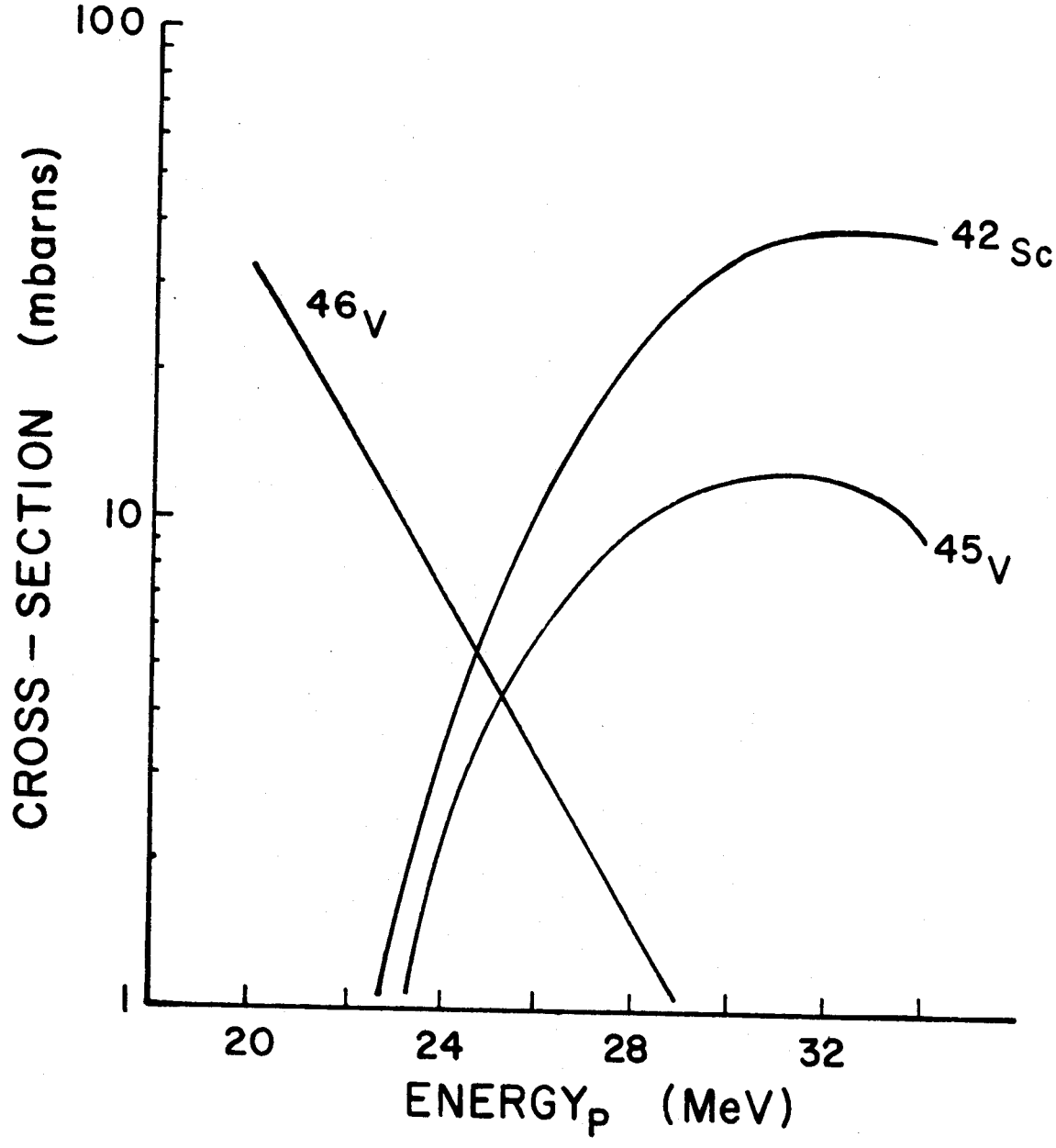

Figure 8-4. ALICE predictions for protons on ^{46}Ti.

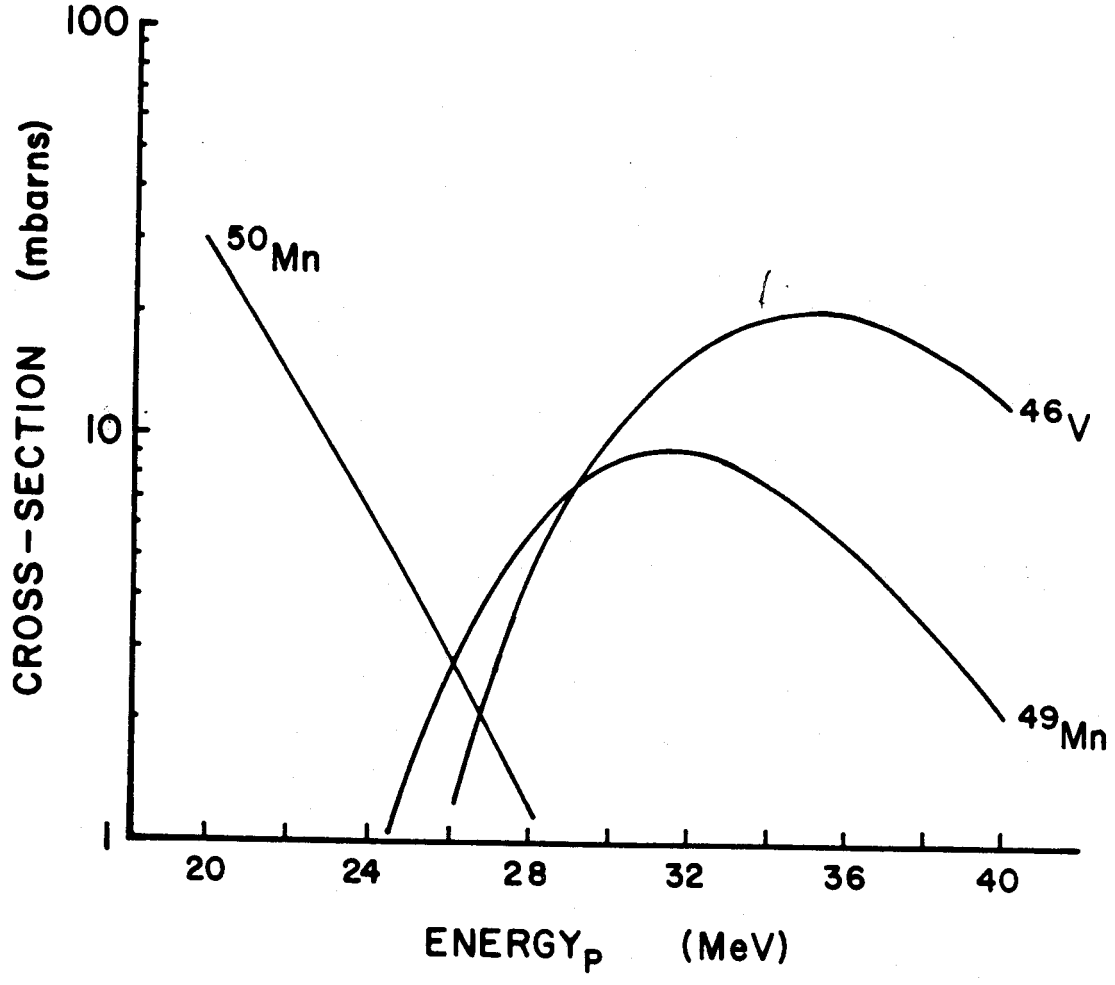

Figure 8-5. ALICE predictions for protons on ^{50}Cr.

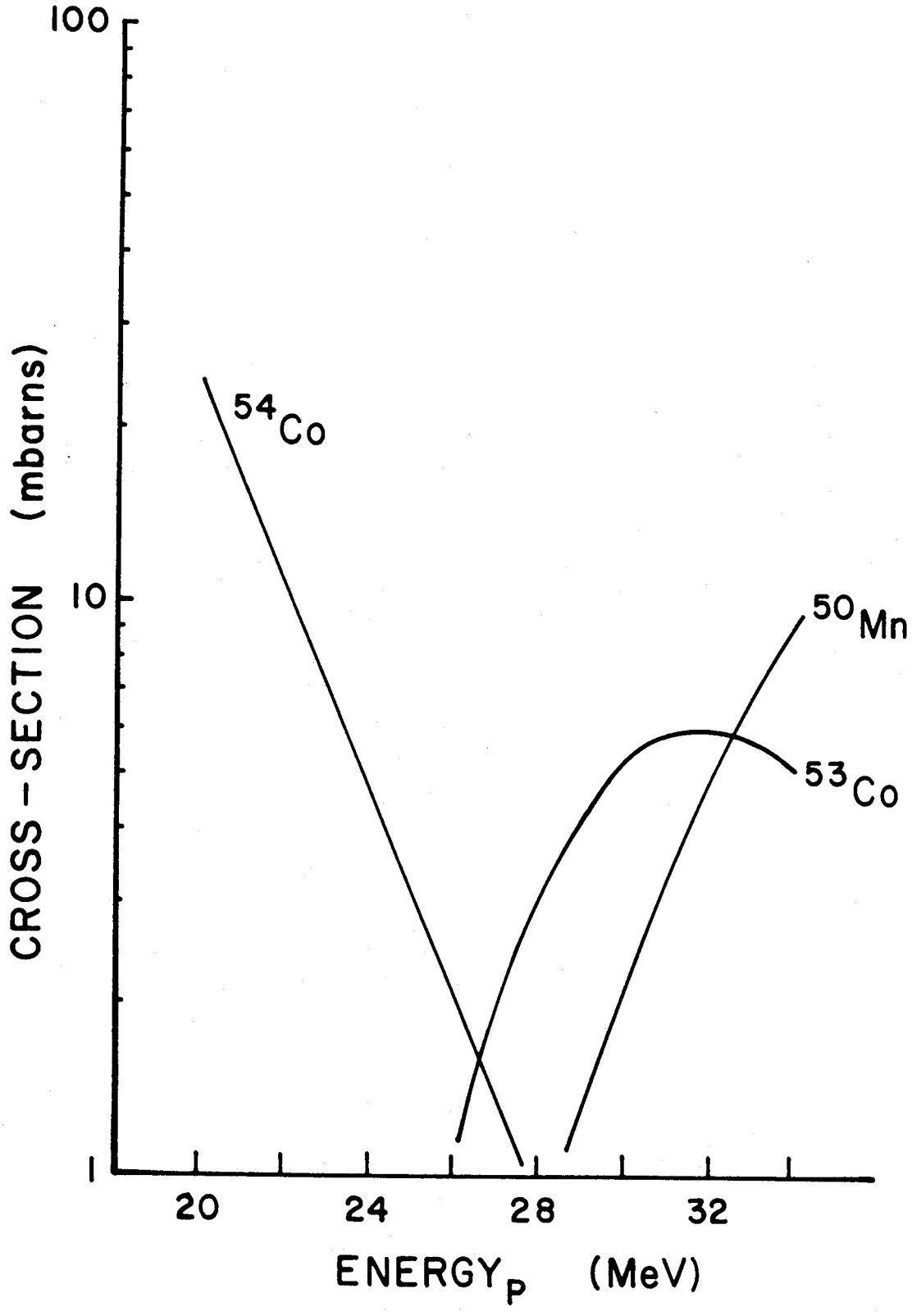

Figure 8-6. ALICE predictions for protons on ^{54}Fe.

Evidently, it is impossible to measure a good half-life for these mirror decays if the decay of the mirror cannot be distinguished from the decay of the impurity. The presence of a shutter in SIEGFRIED made SIEGFRIED suitable for measuring half-lives with changes only in the electronics. One merely needs to add one more parameter to the data, viz., the time of occurrence of the event in relation to shutter closure.. In every case, the impurities have different mass number than the mirror of interest, so SIEGFRIED can unambiguously separate the decays of interest from the impurities.

The first nucleus chosen for study with SIEGFRIED was ^{47}Cr. This was chosen since it should have the longest half-life next to ^{45}V, yet it has only one impurity to deal with. The data were collected using the PDP-11/45 computer and the electronics set-up as shown in Figure 8-7. The 11/45 program lets us view the counts in the ramp spectrum which come from a selectable mass peak and a selectable β-energy region. The set of data so obtained is shown in Figure 8-8, in which the mass peaks are shown on top and the ramps due to each peak are shown below them. The low-energy β-detector counts were removed since they contain 511-keV $\gamma^{\pm}$ from the decay of ^{47}V. It is obvious from the data that we have made ^{47}Cr and that its half-life is about the same as ^{46}V (0.42 sec). It is also obvious that if we desire to get a better estimate of the half-life, we need to collect many more data. Doing so is nearly impossible since it took on the order of 8 hours to collect the data displayed. At this point, SIEGFRIED appears to be too inefficient to do the job. This was very disappointing since this nucleus should be fairly typical in terms of cross-section and

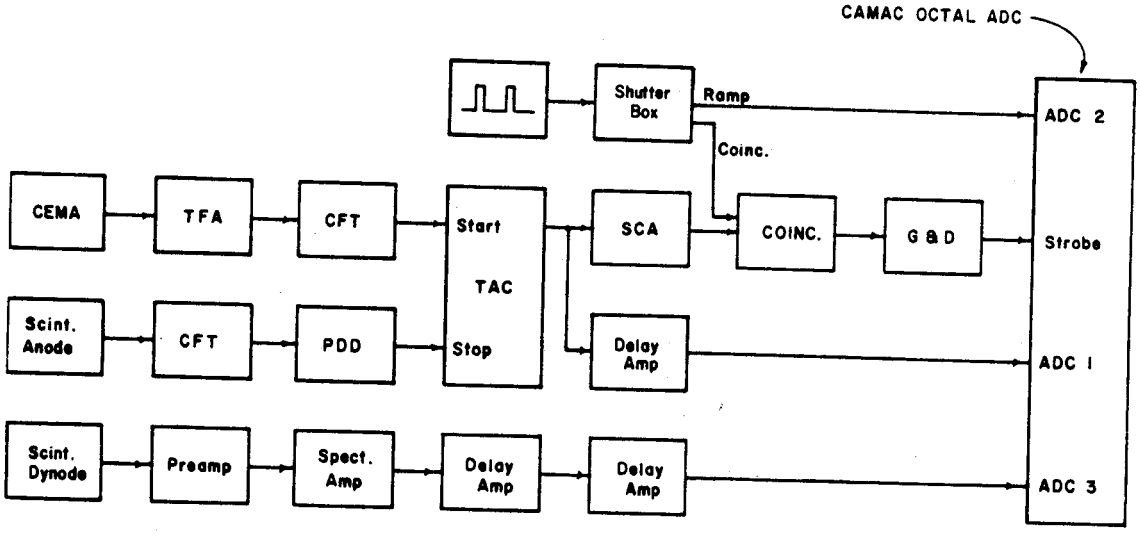

Figure 8-7. Electronics used to collect the data shown in Figure 8-8.

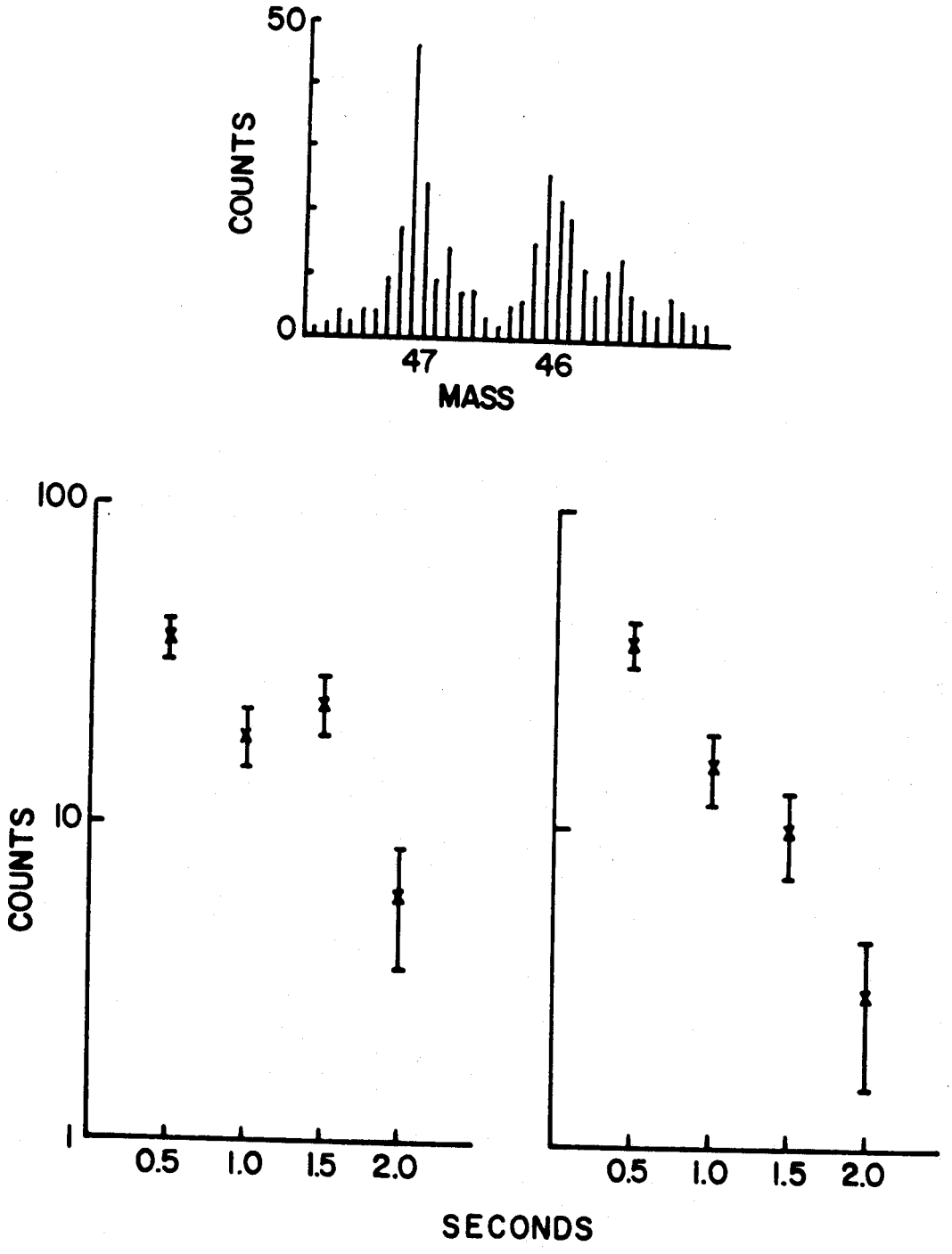

Figure 8-8. Data collected when attempting to measure the half-life of ^{47}Cr with SIEGFRIED.

half-life to what we would like to study with SIEGFRIED. Therefore, a substantial amount of time was spent trying to surmise why SIEGFRIED worked so poorly on this study. The results of these experiments seem to point at the He-jet transport time.

9. SIEGFRIED's EFFICIENCY

The observations and conclusions expressed in this section are not well established and are not well understood. However, it is possible to construct a picture which makes intuitive sense, and this picture will be considered to be accurate until proven otherwise.

The experiments break down into three parts depending upon the operating parameters of the He-jet and whether or not SIEGFRIED is used. The first case uses SIEGFRIED with a 0.8-mm capillary and a He flow rate of 1000 ml/min (STP). In this case SIEGFRIED's vacuum pumps are "comfortable" and SIEGFRIED appears to work very well with the aluminum target. The shortest half-life which has definitely been seen in this configuration is 2-sec ^{26}Si. The cross-section for producing the ^{26}Si is 3 mb as calculated by ALICE, but we have seen ^{25}Al, which has a calculated cross-section of 2 mb. That is the smallest cross-section known to have been seen with SIEGFRIED. The efficiency for this case seems to be very good because the ^{26}Si and ^{25}Al are observable after about half an hour of data collection. Peaks such as ^{23}Mg with cross-sections of several tens of mb appear quickly. Also, very little activity seems to accumulate on the skimmer.

In the second case SIEGFRIED is used with 1.4-mm capillary. The He flow is about 2000 ml/min (STP) and SIEGFRIED's vacuum pumps are on the verge of shutting down. (The pressure at the target must be reduced to enable this capillary to be used.) The shortest half-life definitely seen is 0.42-sec ^{46}V with a production cross-section (calculated) of about 8 mb. The lowest-cross-section product seen is again

^{25}Al. However, in this case the efficiency appears to be very poor. All mass peaks are reluctant to appear (it takes 6 to 10 hours to see a good mass spectrum), and there is significant build up of activity on the skimmer. It seems there is so much gas flow that a great amount of turbulence exists at the skimmer which prevents the activity from going through.

The last case is for using the He-jet alone (without SIEGFRIED) with a 1.4-mm capillary and gas flow of 4000 ml/sec (STP). In this case we have easily seen half-lives as short as 0.2 sec and many other labs report seeing even shorted-lived nuclides. The lowest cross-section seen is not known, but the 0.2-sec half-life activity has an ALICE prediction of about 1 mb.

It has been conjectured by several He-jet experts (e.g., (Ma73)) that the major portion of the He-jet transport time is the time it takes for the target recoils to enter the capillary. This makes intuitive sense because once the recoils are in the capillary they move very fast. The transport from the target to the capillary entrance is accomplished by diffusion and helium flow. This process is slow unless the helium flow is so great that there is a stream of helium flowing across the back side of the target. Thus it seems that the greater the helium flow, the faster the transport. (Note that if one increases the helium flow by increasing the size of the capillary, the in-capillary time remains fairly constant. To decrease the in-capillary time, the capillary must be shortened or the target-area pressure must be increased. Increasing the target-area pressure can lead to choked flow and poor transport if one is not careful (We75).)

The results of the experiments described in the first part of this section seem to agree with the ideas presented in the preceding paragraph. We need a high helium flow rate to get fast transport from the target to the capillary, but we need a low flow rate to make the skimmer work properly, and we need a low flow rate to maintain the vacuum in the TOF chamber. This dilemma leads one to be pessimistic about the value of SIEGFRIED, and forces us to attempt to gain a better understanding of the problem.

One thing that was attempted was to actually measure the transport time with SIEGFRIED. This was done by using the beam pulser to give a sudden pulse of beam on the target. The beam pulser also started a ramp signal which was sampled everytime a γ ray was detected at SIEGFRIED. Unfortunately this gave very inconclusive results because there is no way to quickly wipe off the activity previously collected on the collector. The amount of new activity is so small compared to the old, that the point in time at which new activity appears is very hard to determine.

Another experiment was tried which should measure the in-capillary time. This was identical to the previous experiment except that the CEMA pulses were used to sample the ramp instead of γ-ray pulses. The plasma created by the beam should appear almost instantly when the beam is turned on. Thus the time between starting the beam and detecting the plasma (with the CEMA) should be the transport time. However, it is more likely that the plasma instantly fills the whole target chamber (because of multiple scattering) rather than being localized to the area of the beam spot. Therefore, this should give a

measure of the in-capillary time instead of the whole transport time. The CEMA-gated ramp appears in Figure 9-1. This shows that the in-capillary time is about 600 msec. A calculation based on flow rates, pressures, etc., yields about the same result. Thus it is reasonable to expect the total transport time exceeds 1 sec. If this is true, then a 0.4-sec half-life nuclide such as ^{47}Cr will spend perhaps 3 half-lives in transport, and its effective production cross-section could be reduced by a factor of 1/8. Another mirror decay, ^{55}Ni, $t_{1/2} \approx 0.2$ sec, may spend 6 half-lives in transport making its effective cross-section be reduced by a factor of 1/64.

At this time, the exact transport time is not known; and if it is too long, the remedy is not known. This problem may be the major limitation to SIEGFRIED's utility and should be better understood.

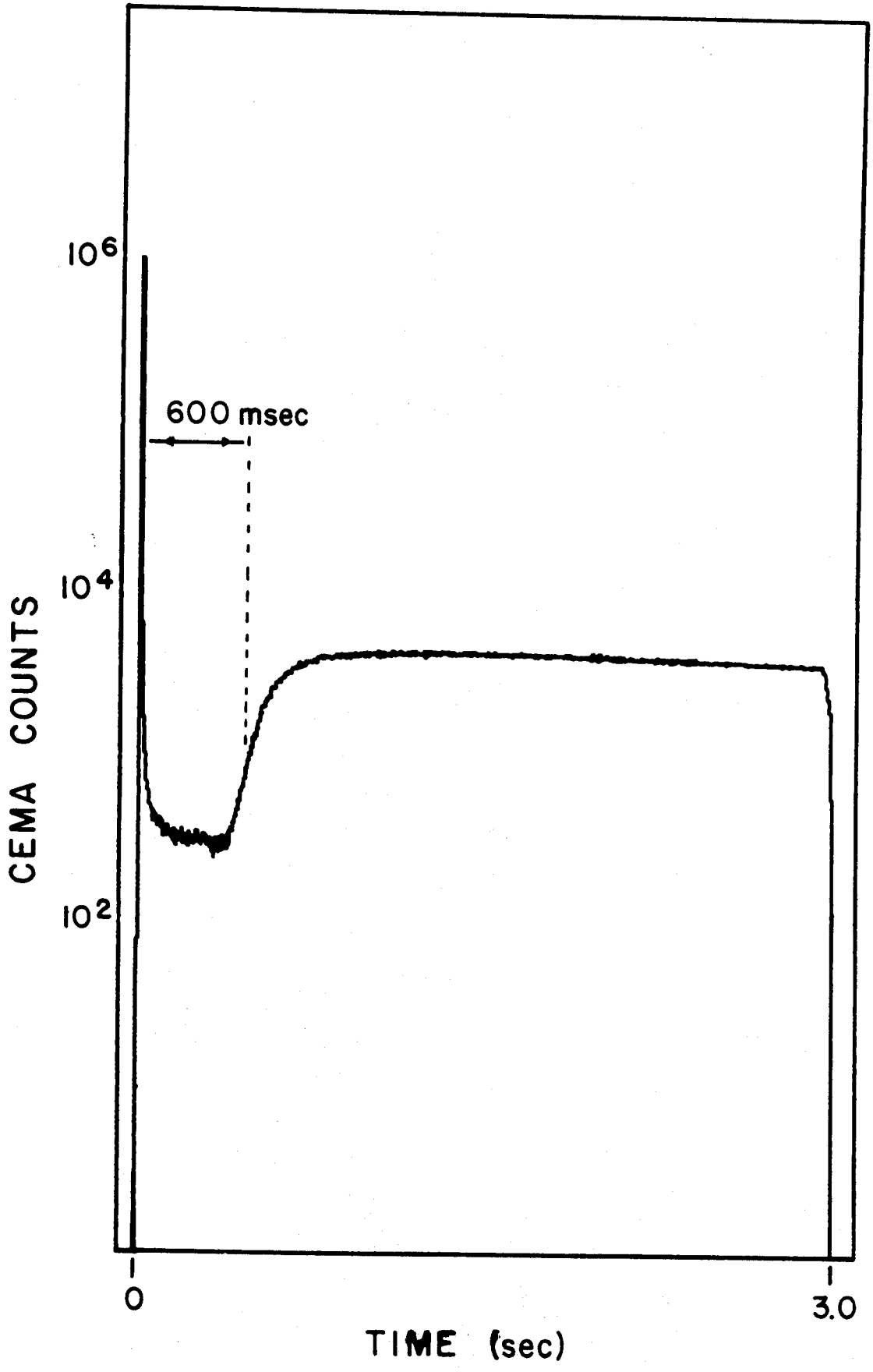

Figure 9-1. CEMA-gated ramp spectrum showing the plasma transport time.

10. THE HALF-LIFE OF ^{47}Cr

In view of the transport problems it seemed hopeless to pursue the mirror β decays any further via SIEGFRIED. However, so much time was invested that it seemed worthwhile to try to finish at least one of the measurements. It was decided to see if SIEGFRIED could confirm the ALICE prediction that ^{47}Cr can be made without making ^{46}V by running at a beam energy less than the Q-value for ^{46}V. If so, one can measure the half-life of ^{47}Cr without SIEGFRIED. It may seem like redundant information to check out the ALICE prediction because certainly if one runs below the Q-value for ^{46}V, it can't be made. However, it is important at MSU for two reasons. First, we arrive at the proper beam energy by degrading a 70-MeV ^{3}He beam down to the desired 16 to 17 MeV using an aluminum absorber. This is done because the MSU cyclotron runs much more reliably at the higher energies (with the rf tuned to the first harmonic) than it does at the lower energies (rf tuned to the second harmonic). (In fact it won't run at all below 17 or 18 MeV.) When we degrade by such a large amount there is always the possibility that straggling will permit some ^{3}He to arrive at the target with energy greater than the Q-value for making ^{46}V. The straggling is difficult to calculate when the energy loss in the absorber is as great as in our case. The second point is that the cross-section for making ^{47}Cr will be falling rapidly as we go lower in energy. It would seem worthwhile to confirm that we still make an observable amount of ^{47}Cr at the lower energy.

Figure 10-1 shows the results with SIEGFRIED when we run with 22-MeV ^{3}He and 16-MeV ^{3}He. Sure enough, the ^{46}V goes away and the ^{47}Cr stays. It is too bad that the efficiency is so low for this case because the statistics are not good enough in Figure 10-1 to say for sure that there is absolutely no ^{46}V being made. Nonetheless, it can be determined that if there is ^{46}V being made, it constitutes less than 5% of the amount of ^{47}Cr that is being made.

Since ^{47}Cr is now known to be the only high-energy β emitter being made with the beam and absorber used when taking the data for Figure 8-1, one can use the same beam characteristics to study ^{47}Cr with the He-jet alone; just collect some activity and watch the high-energy β counts decay away. A chopper was constructed which consists of a spinning plexiglas wheel. The He-jet is aimed such that it sprays through a slit in the wheel when the wheel is in a particular position, and it sprays on the plexiglas at all other times. The wheel is adjusted so that the He-jet is on for about 2 half-lives and off for about 7 half-lives. The time base is provided by the 100-MHz oscillator of the PDD. This oscillator is divided digitally by 10^{6} to give an accurate 100 Hz square wave. (The 100-MHz rate is checked against a crystal-controlled frequency counter accurate to at least 1 ppm.) The 100-Hz signal drives a sequencer which routes the β signal into different spectra in the computer depending on the number of oscillator counts. The sequencer is kept in synchrony with the chopper by a little reed-relay and magnet arranged to reset the sequencer at the moment the He-jet is cut off. The activity is collected on a paper tape in front of a plastic scintillator. Just before a new spot of

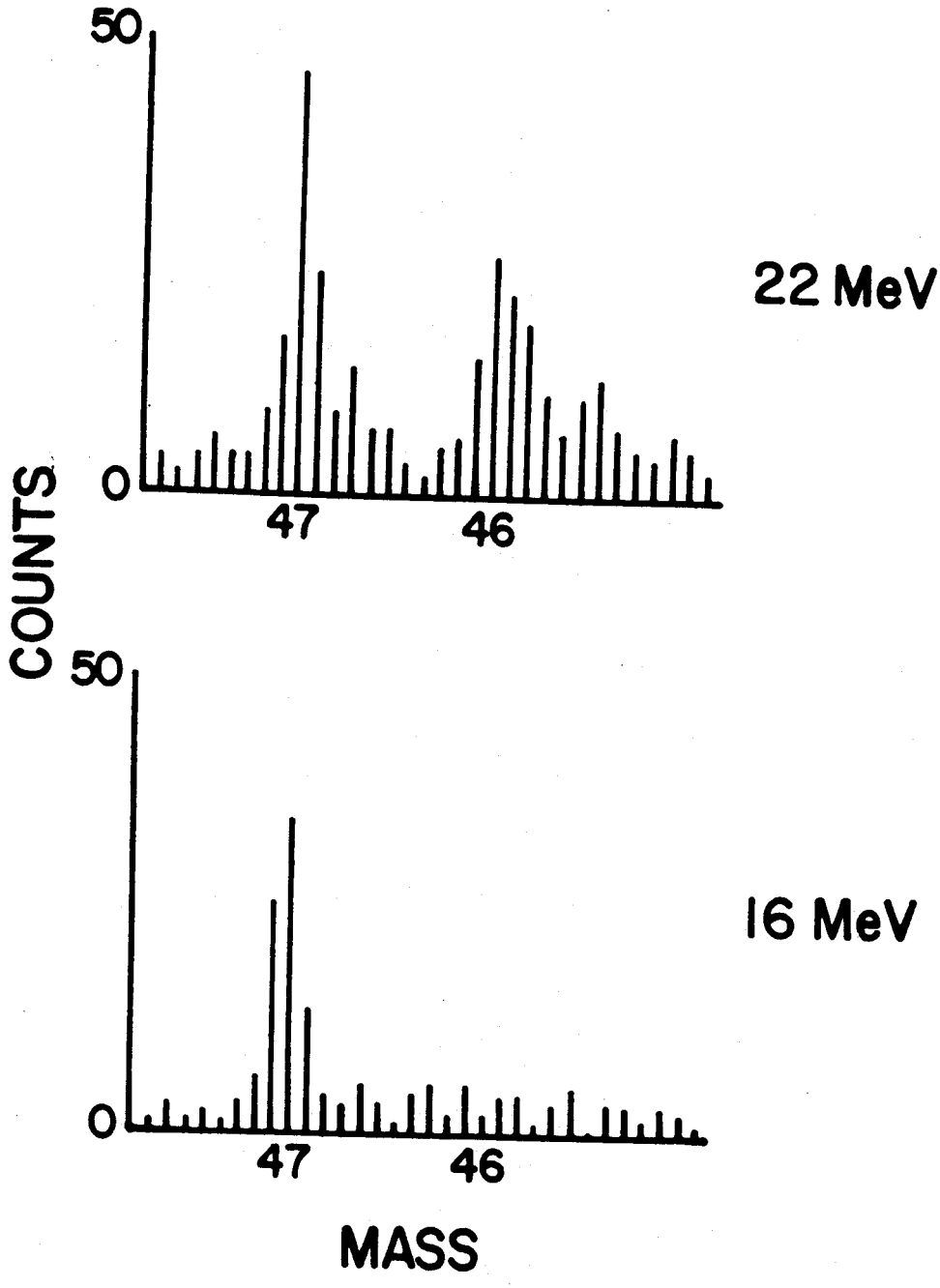

Figure 10-1. Mass spectra obtained with 22-MeV and 16-MeV ^{3}He on ^{46}Ti.

activity is collected, the tape advances several inches to remove the long-lived activity. A schematic of the experiment appears in Figure 10-2 except that the paper tape is not shown. A total of 13 spectra were taken in which each spectrum lasts for exactly 250 msec. A line frequency pulser was fed into the pre-amp of the plastic scintillator to give dead time correction. Some of the spectra are shown in Figure 10-3. It is easily seen that the high-energy β counts are decaying away in the time scale represented, and these are attributed to ^{47}Cr. The low-energy counts do not change much because they result from 511-keV $\gamma^{\pm}$ which is not stopped by the plexiglas wheel. These counts come from all the activities being made and are very constant over several chopper cycles. Most of them are from ^{47}V, which has a 30-min half-life and some are from ^{47}Cr. As long as the beam is relatively constant, these ^{47}Cr $\gamma^{\pm}$ are constant, but a slightly better fit to the data is obtained if the low energy counts are excluded in making the fit. Accordingly, a low-energy cut-off channel was designated and all the counts above this channel were added to give the number of counts for that time interval. This low-energy cut-off channel was varied until the best fit was obtained. The cut-off in energy finally chosen is close to 1 MeV and is shown in Figure 10-3 by the arrow. The peak at about 7 MeV is the pulser.

The fits were calculated by the computer code KINFIT which was written in the MSU Chemistry Department (Dy71). This program is a non-linear curve fitting routine which lets one solve for several parameters at the same time. The data and fit for ^{47}Cr are shown in Figure 10-4. A nice feature of the KINFIT program is the ability to change

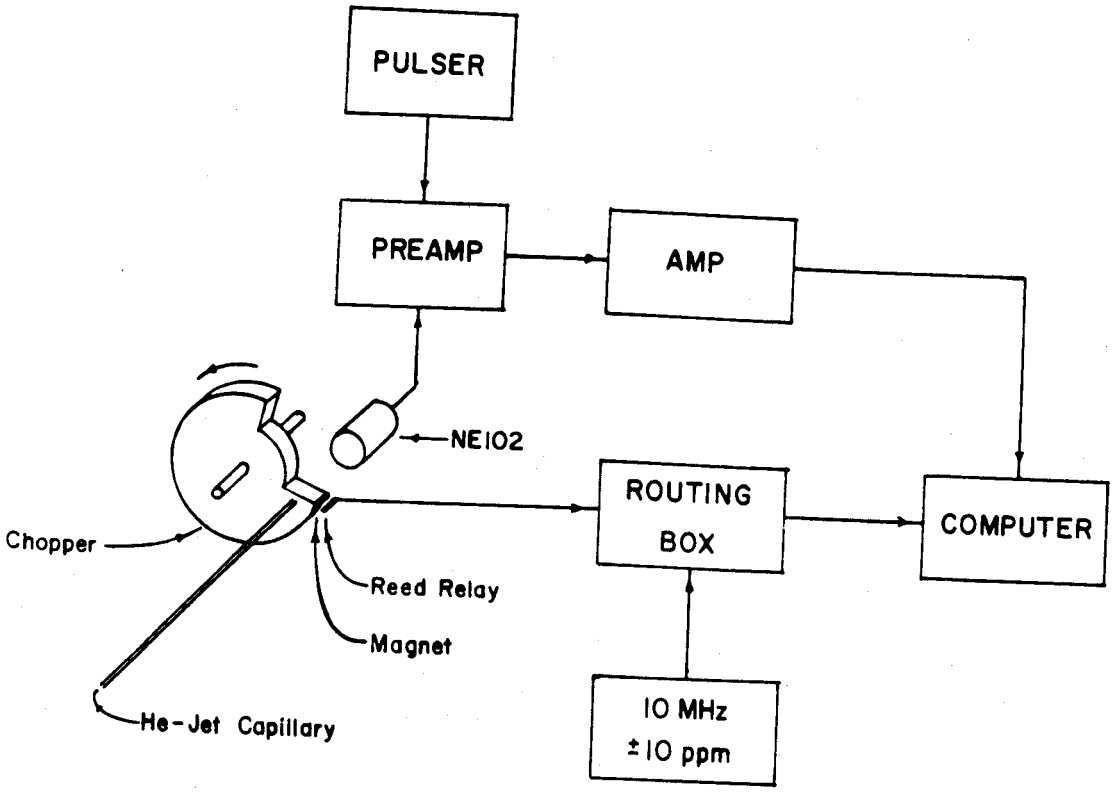

Figure 10-2. Schematic diagram of the chopper system used to measure the half-life of ^{47}Cr.

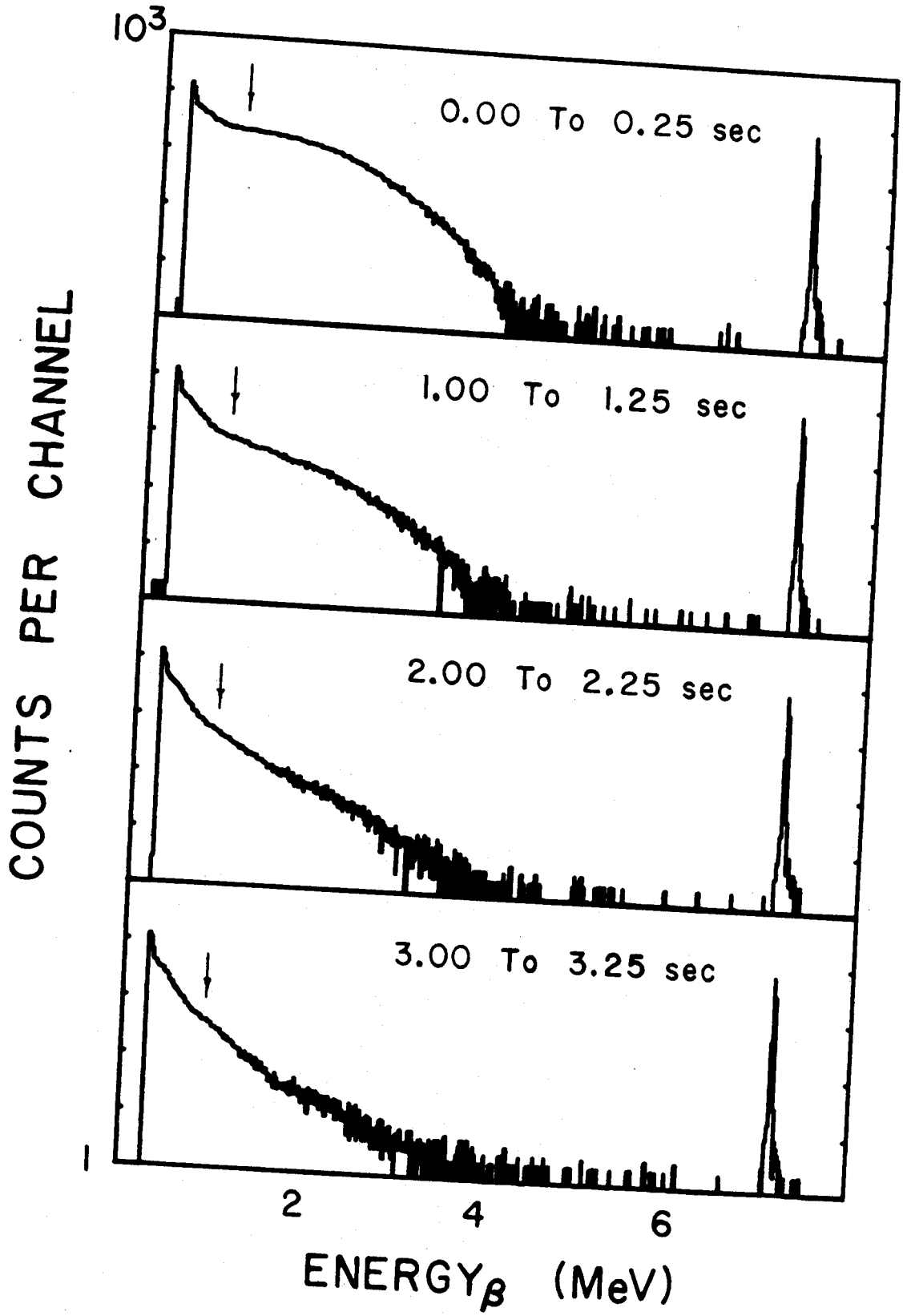

Figure 10-3. Some of the β spectra from the ^{47}Cr half-life measurement.

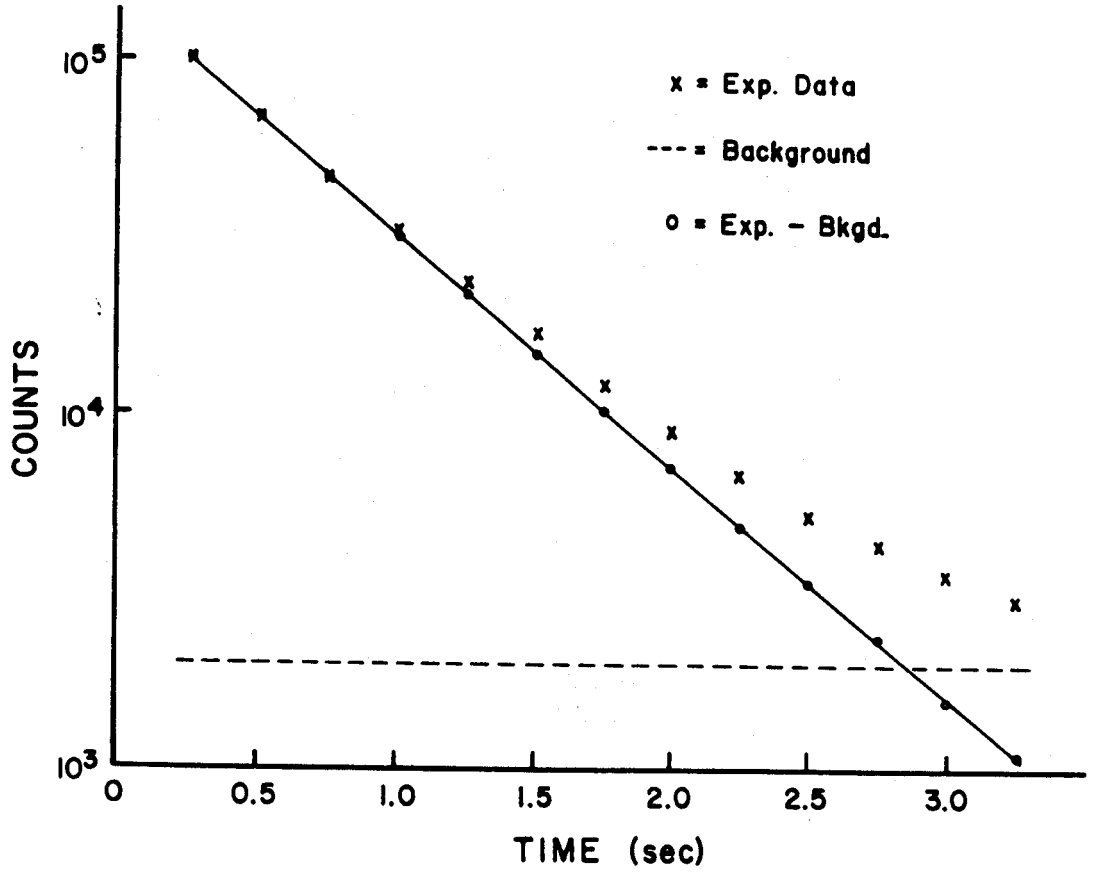

Figure 10-4. The data and the fit for the ^{47}Cr half-life measurement.

the equation to account for various amounts of ^{46}V that might be present. The results of this analysis are shown in Table 10-1. It is now an asset to have the half-lives of ^{47}Cr and ^{46}V so close together because the half-life calculated for the data is not changed very much by the addition of moderate amounts of ^{46}V.

Table 10-1

^{47}Cr Data Analysis Using KINFIT
in which the Equation Solved is:
$COUNTS = A \times \exp(-\lambda t) + Const \times \exp(-\lambda_{^{46}V} t) + B.$

Const	$t_{1/2}$
0	460.0 msec
1%A	460.8 msec
2%A	461.2 msec
5%A	462.4 msec
10%A	464.6 msec

As a test of the chopper experiment, the half-life of ^{46}V was measured. This was previously measured elsewhere and found to be 423 ± 2 msec (Ha74). Our value is 420 ± 3 msec giving very good agreement with the earlier number, and giving confidence in the MSU system.

Our final value for the half-life of ^{47}Cr is 460 ± 1.5 msec. This gives a log*ft* of 3.63. Having finished ^{47}Cr, it was decided to try to measure ^{55}Ni with the chopper. This was done, and its half-life found to be 219 ± 6 msec. Needless to say, with a half-life this short, we have not yet confirmed this with SIEGFRIED.

11. β-RECOIL ENERGY DISTRIBUTIONS

Once it was clear that many of the β recoils were leaving the collecting surface with most of their initial energy, it became natural to wonder if SIEGFRIED might be used to measure the energy distributions of such recoils. Such measurements would be valuable to β-decay theory because, among other things, they would enable one to deduce the mixing ratios of the Fermi (F) and Gamow-Teller (G-T) components of the decay. The energy distributions of the recoils from F and G-T decay can be calculated and appear in Figure 11-1 (Wu66).

We saw earlier how the ORE_{max} in SIEGFRIED leads to a transformation of the actual distribution shape to the shape observed in the mass spectrum. It would seem that one merely needs to reverse the calculation to get the recoil distribution from the mass shape. This is not easily done because of two problems which are a result of the ESPG. Remember that TRE = PRE + ORE (see pages 20 and 21). It is PRE which causes the shift in TOF and the resulting wide mass peaks, while it is the TRE distribution we hope to measure. Hence, when ORE_{max} is very small, we see that TRE ≈ PRE, and the mass-peak shape is actually the TRE shape within a small error (once the fall-off in efficiency is accounted for). Since ORE_{max} is only about 0.8 eV when the ESPG is turned off, and since the TRE values are between zero and several hundred eV, the error in assuming TRE to be PRE is actually quite small.

However, when the ESPG is turned on, meaning ORE_{max} is large, the TRE values become "smeared" between all combinations of PRE and ORE, where ORE may now be a significant fraction of TRE. In short, this

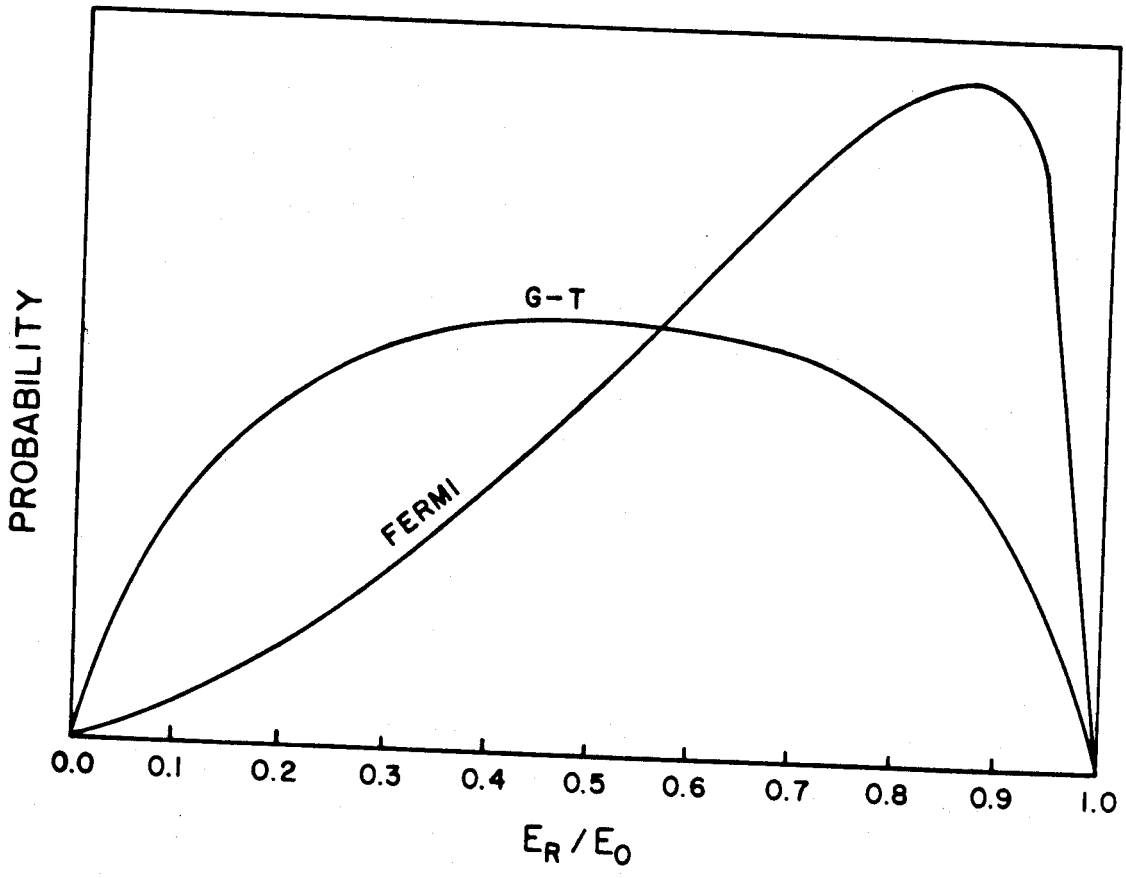

Figure 11-1. Calculated β-recoil energy distributions.

simply means that there is insufficient information in the mass-peak shape to determine the TRE spectrum unless the ESPG is turned off.

The other ESPG problem is the field perturbation caused by the end of the ESPG wire nearest the collector. This perturbation has the result of adding to the accelerating voltage from zero to the full ESPG voltage, depending on how close the recoil's trajectory comes to this end of the wire. This problem is somewhat solvable by attaching the beginning of the ESPG to a grid so that all recoils will experience the same increase in energy regardless of their path. (There would still be a perturbation at the edges of the grid.) In view of the problem already discussed, this hardly seems to be worth the effort if done merely to study the recoil distributions. However, since the perturbation no doubt causes some of the TOF spread shown at higher ESPG voltages (page 32), it may be worthwhile to consider the grid as a means to improve not only the resolution, but also the efficiency (since it may permit higher ESPG voltages to be used). Of course, if this is done, the ESPG power supply will have to be made stable to within about 0.1 V, which is the approximate stability of the HV supply.

As a test of the use of SIEGFRIED for measuring recoil-energy distributions, it was decided to look at the mass shapes for a known F decay and a known G-T decay to see if we could come up with the proper distributions. Finding and making nuclei which decay by a pure F interaction is no problem. We have frequently made ^{26}Al which is such a decay. Finding a pure G-T decay is a little harder, but a good choice seemed to be ^{18}F which is a 1^+ to 0^+ transition and thus pure G-T. One way to make ^{18}F is to use the reaction ^{20}Ne$(p,2pn)^{18}$F.

Since neon is a gas, it presents somewhat of a target problem. By using the He-jet, this first appeared to be a trivial problem because it was thought that we could merely substitute neon for helium as the carrier gas. However, the density of neon causes an increase in the Reynolds number for the jet, making the flow tend to be turbulent instead of laminar. This means that the activity tends to stick to the capillary walls instead of being transported. In fact, the "Ne-jet" clogged the capillary with cluster material after a few minutes of operation.

The next attempt was to try mixing neon and helium with hopes that the helium would bring the density of the mixture down enough to assure laminar flow. This seemed to work reasonably well when the mixture was 50% neon and 50% helium. (A small amount of benzene was still used to generate the clusters.)

Once the target and transport problems were solved, we found that SIEGFRIED just does not have a high enough efficiency (without the ESPG) to make the measurement feasible. Several hours of data collection resulted in peaks which were barely discernable above background.

At this point it was decided to turn the ESPG back on, and to set the HV to a value high enough to get reasonable efficiency, yet low enough to keep ORE_{max} from wiping out any recoil-energy information. When this was done, the set of data shown in Figure 11-2 was collected. What we hoped to see was a qualitative difference in the peak shapes for ^{26}Al and ^{18}F. As one can readily see, we got more than we hoped for - the ^{18}F has essentially no tail, while the ^{26}Al has a sizable tail. In addition, the ^{29}P peak, a result of a $1/2^+$ to $1/2^+$

transition, is also lacking a tail. Unfortunately, the peak-shape difference is more drastic than we can explain. G-T transitions should still have tails; they should just be somewhat different tails than F transitions. The difference observed in Figure 11-2 makes one wonder if SIEGFRIED is displaying sensitivity to some other factor, e.g., chemical effects at the collector. The chemical-effects explanation is not very satisfying since recoil energies of several-hundred eV should be well above the strengths of chemical bonds. However, other explanations are difficult to conjecture, and we would like to believe that the difference has something to do with the type of decay rather than resulting from some artifact in SIEGFRIED. At this point, the problem must remain unanswered, but there still seems to be hope that SIEGFRIED can be useful in this area of β decay.

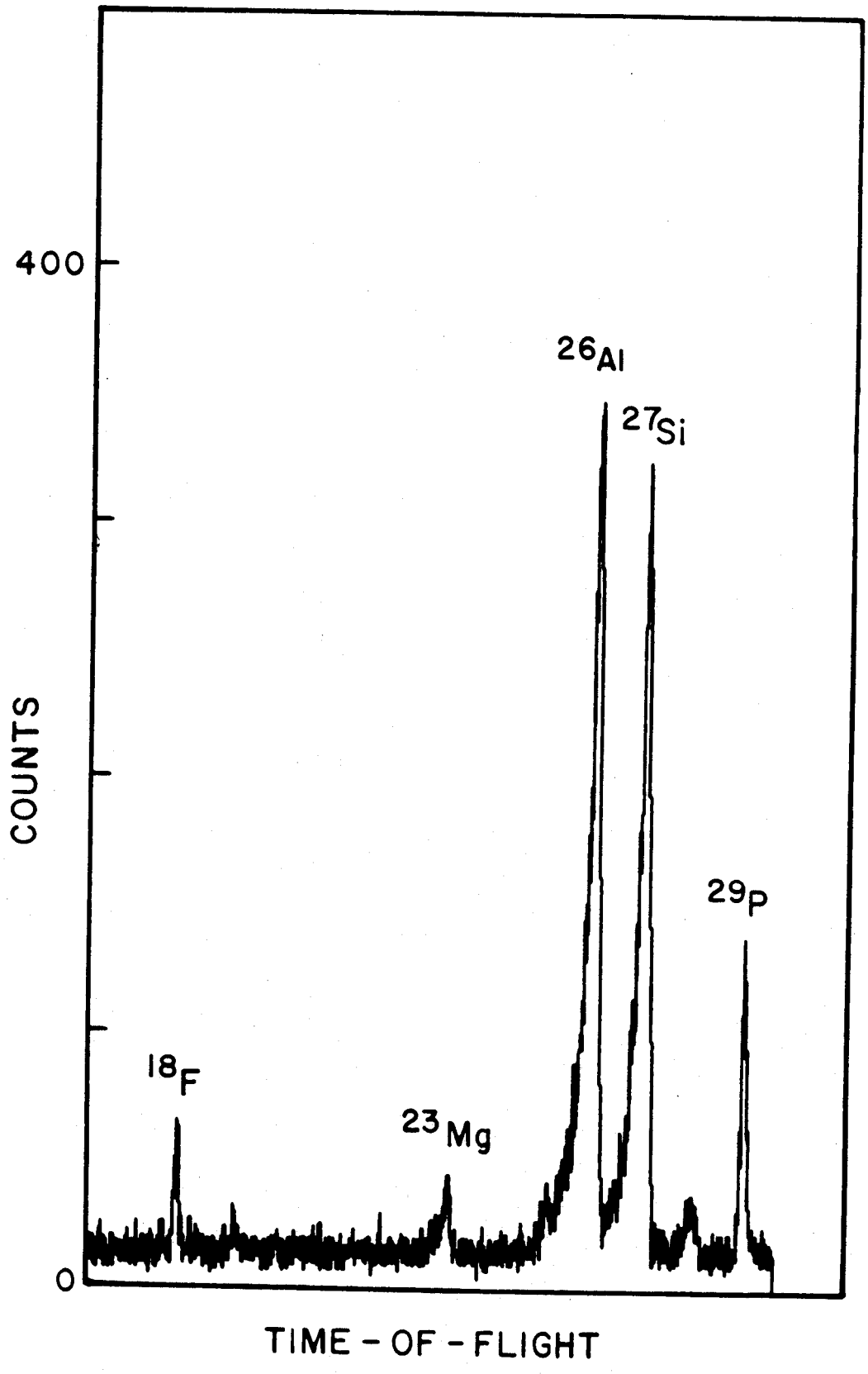

Figure 11-2. TOF spectrum from 32-MeV protons on ^{20}Ne and 20-MeV protons on ^{27}Al. HV was 6 kV to keep ORE_{max} low.

12. CONCLUSION

At this time, it may appear difficult for one to determine whether he should be pessimistic or optimistic about SIEGFRIED. The main reasons for being pessimistic are the transport time and the overall efficiency. However, the poor transport time is clearly a He-jet problem and does not really reflect poorly upon the basic idea behind SIEGFRIED. There are hopes of correcting this with a better skimmer and/or a shorter capillary. Laboratories contemplating building a similar machine would do well to plan the vacuum system much more carefully than we did. With good transport the efficiency is not really so poor, and preliminary γ-mass coincidence experiments indicate that, with the present system, we can obtain γ-mass coincidences for the stronger γ rays in about 8 hr of data collection.

There are many reasons to be optimistic. First of all, the system works and does not have the chemical specificity problems that the magnetic systems have with their ion source. The results given in this dissertation show that SIEGFRIED is a viable alternative to the magnetic systems, especially when one considers the cost. If β-recoil information should prove to be obtainable with SIEGFRIED, a new area of unexpected applications could easily result.

In short, SIEGFRIED is in the uneasy position of being a usable tool, yet still under development. Only concentrated attempts at specific experiments can truly estimate its value.

APPENDICES

APPENDIX A

SIEGFRIED's VACUUM SYSTEM

Description

The vacuum system is the bulk of SIEGFRIED's size and the bulk of its cost. This is because the vacuum must be kept at about 10^{-6} torr even though helium is flowing in at a fairly large rate. The vacuum must be good for two reasons: it must be better than 5×10^{-5} torr so that the mean-free-path of the recoils will be comparable to the flight length; and it must be about 10^{-6} torr before the CEMA can be used properly. If the vacuum at the CEMA is worse than 10^{-6} torr, there is an ion-feedback problem which causes a background CEMA rate, and a shorter life for the CEMA. If the vacuum should get as bad as 10^{-3} torr, then there is a possibility of arcing (which will immediately destroy the CEMA).

When the 0.8-mm capillary is used, the helium flow rate is about 1000 ml/min (STP) which is 16.7 ml/sec (STP). This becomes about 1.3×10^{7} l/sec at 10^{-6} torr, and diffusion pumps with this capacity do not exist. Therefore, differential pumping across a skimmer must be done. The He-jet enters the first of two vacuum boxes and is aimed at a small hole at the apex of a cone. The hole leads into the second vacuum box which is the TOF box. An Edwards 18B4-booster pump provides the vacuum in the first box and can provide pumping speeds of about up to 6400 l/sec for helium. This means that the first vacuum box (i.e., the skimmer box) will be maintained at about 2×10^{-3} torr. The hole is about 1.3 mm in diameter which means that the flow rate through it will

be 0.16 1/sec at 2×10^{-3} torr = 320 1/sec at 10^{-6} torr. Thus, to keep the vacuum at 10^{-6} torr in the TOF chamber, the diffusion pump must handle at least 320 1/sec. Actually the vacuum at the skimmer will be worse than 2×10^{-3} torr because the capillary is so close. If it is as bad as 10^{-2} torr, then the TOF pump must handle 1600 1/sec. A 25-cm diffusion pump was installed which is rated at 2000 1/sec when baffled with a LN_2 trap. Because the flight tube offers an impedance to the gas flow, an additional 10 cm diffusion pump was attached beneath the CEMA.

The 18B4-booster is fore-pumped by a 95-1/sec Roots-blower in turn pumped by a 7-1/sec vane pump. The 25-cm diffusion pump is fore-pumped by a 25-1/sec vane pump. The 10-cm diffusion pump is fore-pumped by a 5-1/sec vane pump, which is also used for roughing the system. A drawing of the vacuum system is shown in Figure A-1. The fore-pumps are perhaps a little poorly chosen, but are arranged as they are because of availability. Specifically, the 25-1/sec vane pump is larger than necessary for the 25-cm diffusion pump and the 7-1/sec vane pump is a little too small for the 95-1/sec blower. However, with the 0.8-mm capillary, the system works well. Typical vacuums with 1000-ml/min (STP) helium flow are:

Skimmer chamber	1×10^{-2} torr
TOF chamber	6×10^{-6} torr
CEMA	2×10^{-6} torr
25-cm fore-line	2×10^{-2} torr
18B4 fore-line	2×10^{-1} torr
10-cm fore-line	5×10^{-2} torr

All of these values are quite acceptable.

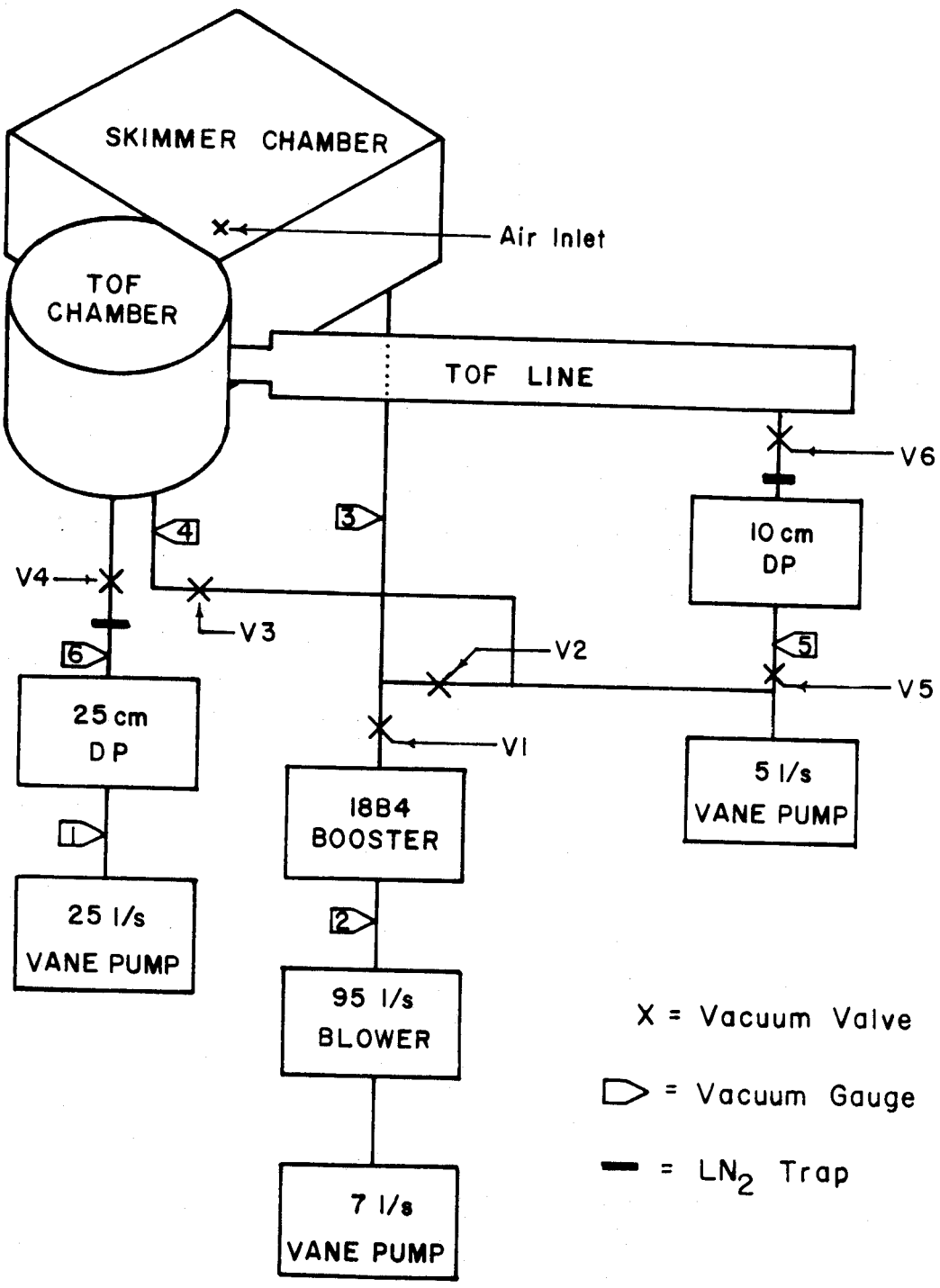

Figure A-1. SIEGFRIED's vacuum system.

Vacuum Interlocks

The vacuum control panel is provided with interlocks to help prevent equipment damage if things go wrong or when buttons are pushed out of sequence. The interlocks will now be listed.

Pump Name	Conditions for Pump to be Turned On
25-cm DP	water on 25-l/sec pump on gauge 1 satisfied (200 mtorr)
18B4 booster	water on 95-l/sec blower on †gauge 2 satisfied (≈500 mtorr) *water temperature ok *boiler temperature ok
10-cm DP	water on 5-l/sec pump on gauge 5 satisfied (≈200 mtorr)
95-l/sec blower	water on 7-l/sec pump on gauge 2 satisfied (≈500 mtorr)
25-l/sec pump 7-l/sec pump 5-l/sec pump	no interlocks other than circuit breakers

†This can be pushed to 2 torr if necessary but caution is called for.

*Water temperature must be less than ≈35°C. A thermometer is in the return line but it is not connected to the interlock. The interlock is a switch welded to the side of the pump. The boiler switch is welded to the boiler.

Valves	Condition to Open
V-1	gauge 3 satisfied (≈500 mtorr) V-2 closed
V-4	gauge 4 satisfied (≈300 mtorr) V-3 closed
V-6	gauge 4 satisfied V-5 open
V-5	V-2 and V-3 closed
V-2	V-1 closed
V-3	V-4 closed

SIEGFRIED Pump Down

1. Turn cooling water on for all pumps. (Do not turn on 25-cm quick cool.)
2. Turn all pumps on. (V-5 open; all others closed.)
3. If diffusion pumps (18B4 Booster, 25-cm DP, 10-cm DP) were off, then you must now wait 1 hour for them to warm up.
4. Fill traps on 25-cm DP and 10-cm DP with liquid nitrogen.

   25-cm through the funnel

   10-cm through hose with forced air
5. Make sure air inlet (on top of skimmer) is closed.
6. Close V-5.

   Open V-2.

   Open V-3.

7. Watch skimmer vacuum (gauge 3).

   When below 500 mtorr: Close V-2.

   Open V-1.

8. Watch TOF vacuum (gauge 3).

   When below 300 mtorr: Close V-3.

   Open V-4.

9. Open V-5.

10. Open V-6.

11. Turn on Penning gauge (gauge 6).

    When 10^{-5} scale is usable, then it is OK to start CEMA, ESPG, Spellman HV.

12. Turn Penning gauge off.

13. Fill traps with LN_2 again.

    Refill 25-cm every hour at first, then every 2 hr once cold.

    Refill 10-cm every 2 hr at first, then every 10 hr once cold.

    (It takes 2 or 3 fillings before traps really cool down and begin to hold liquid for reasonable times.)

14. Take data.

Note: Rough down (steps 7 and 8) will not work if He is flowing. It will work better if the capillary is attached to the He-jet as opposed to sucking in air. At any rate, this is a slow step requiring 3-4 min to rough down.

Shutdown and/or Bringing SIEGFRIED up to Air

1. Turn He off.
2. Turn CEMA off.
3. Turn Spellman HV off.
4. Turn ESPG off.
5. Close V-6.

   Close V-4.

   Close V-1.
6. Confirm: All valves closed except V-5.
7. Open air inlet (on top of skimmer), it now takes about 5 minutes.

   (Skip step 7 if shutting down.)

(To get back down to vacuum, go to pump down directions and start with instruction #5.)

To shutdown, continue:

8. Turn off: 18B4 Booster,

   95 l/s Blower,

   25 cm DP,

   10 cm DP.
9. Wait 1 hour or longer.
10. Turn off all cooling water. (This can be done the next day; just remember to do it or you'll waste a lot of water.)
11. You're finished.

Note: Mechanical pumps stay on all the time, unless they require maintenance.

APPENDIX B

THE CEMA

Description

The CEMA (Channel-Electron-Multiplier-Array) actually consists of two CEMA's stacked to form a "Chevron" detector. Chevron detectors can be purchased already assembled, but we assembled our own since it was cheaper to do so.

The CEMA operates similar to a photomultiplier tube except it is much smaller and has a much faster response. It is used as a windowless detector and thus requires a very high and very clean vacuum. The several-keV heavy ions created by the HV in SIEGFRIED are nearly the optimum particle for CEMA detection and the efficiency is high. The actual theory of operation is clever but will not be discussed here because it is discussed elsewhere (e.g., (Wa73) or (Gr75)).

SIEGFRIED's Chevron consists of two 2.5-cm diameter CEMA's, one with 0° bias on the channels and the other with 5° bias. They are separated by a stainless steel ring 0.05 mm thick.

The schematic of the CEMA electronics is shown in Figure B-1, and the schematic of the emitter follower is shown in Figure B-2. The ORTEC 459 power supply is used since it has a continuous voltage adjustment and since it has a remote shutdown feature which can be interlocked to the vacuum system. The back surface of the CEMA is held at -300 volts to facilitate electron transport to the collector. This could be done by holding the collector at +300 volts, but then the emitter-follower would have to float. The -300 volts is kept by the

Zener diode in the bias circuit. However, the CEMA draws such little current (5 μA) that the diode is not in the Zener region unless a parallel resistance is put across the CEMA to draw more current through the diode. The bias circuit then draws so much current that the voltage drop across the internal series resistance of the ORTEC 459 is appreciable and the voltage pot no longer indicates the true voltage across the CEMA. The microammeter is inserted so that one can watch the CEMA current while advancing the voltage. It should increase smoothly as the voltage is increased and should yield proper operation when up to about 5 μA. If the voltage is increased, the ion feedback region can be easily seen since the microammeter suddenly jumps by about 1 or 2 μA when the feedback begins. To protect the CEMA, it must be operated below that threshold. Since the ORTEC 459 and the CEMA are very reproducible in operation, a "cook-book" operation procedure can be followed. This procedure will now be given.

CEMA Recipe

Use ORTEC 459 power supply MSU #CU2098. Follow pump down instructions and achieve a vacuum better than 10^{-5} torr as read by the vacuum gauge labeled #6 (the Penning gauge). Valves V-4 and V-6 are interlocked to the 459 power supply and must be open. If the vacuum should go bad they may react fast enough to save the CEMA. They are not intended so much as failsafes as they are to prevent sleepy experimenters from pushing the wrong buttons.

1. Achieve a good vacuum.

2. Slowly increase 459 output until pot reads 2700 volts negative (not actually 2700 volts).

   Watch CEMA current while doing this. It shouldn't jump and it shouldn't exceed 6 μA. If it does, something is wrong - discontinue.

3. The CEMA should now be working.

To use a different power supply (not recommended) or to check CEMA performance (periodically recommended) use the following procedure:

1. Achieve vacuum.
2. Increase negative voltage slowly while watching CEMA current.
3. When up to 4.5 μA of CEMA current, watch emitter-follower output on a scope. (Always terminate emitter-follower in 50 Ω.)
4. Increase voltage until average pulse height is 0.05 V, but avoid the ion feedback region by keeping CEMA current less than 6 μA. (These pulses are very fast and are negative. They should have about 5 ns rise time and 50 ns fall time.)
5. Set TFA so that output into 50 Ω is about 1 volt.

It is easy to get CEMA pulses without the cyclotron. The ESPG can guide Penning gauge ions to the CEMA.

1. CEMA on.
2. Penning gauge on.
3. ESPG manual and negative.
4. Accelerating HV off.

Count rate should be 300-5000 counts/sec depending upon the vacuum at the Penning gauge.

Whenever V-4 and V-6 are open, try to keep the LN_2 traps cold to stop backstreaming from reaching the CEMA. The trap directly beneath the CEMA is most important.

Emitter-Follower Note

The emitter-follower is a very simple circuit, but the values of three components are important. The transistor is chosen by trial to be as fast as possible. A good choice seems to be 2N4122. The 39-Ω output resistor is for impedance matching and the 0.1-μF capacitor (in conjunction with the 50-Ω terminator) provides the proper decay constant.

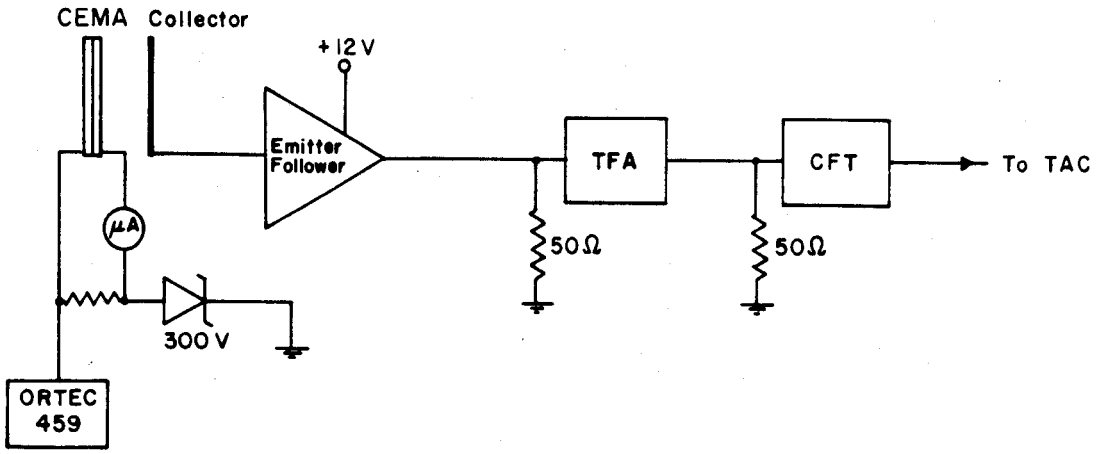

Figure B-1. Schematic of the CEMA electronics.

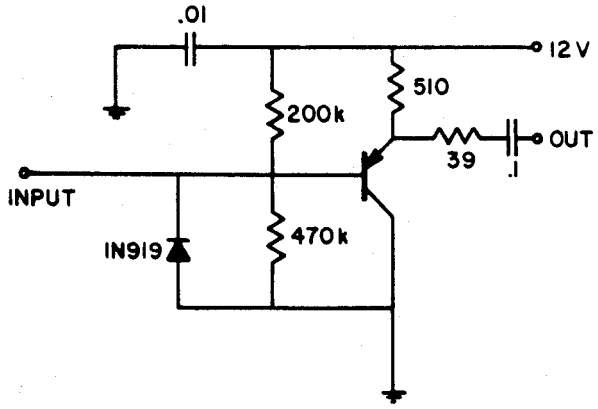

Figure B-2. Schematic of the emitter follower.

APPENDIX C

THE SHUTTER BOX

Description

This box controls the shutter and serves as the control center for functions which relate to the shutter. The overall view of its use appears in Figure C-1. To check for proper operation, hook up as in Figure C-1 and start the pulser. The LED should begin to blink. Unplug the shutter and the LED should quit blinking. (The failsafe prohibits the LED if the shutter does not close.) If it passes these tests, the shutter ought to be working properly. It might also pay to go to SIEGFRIED and try to hear the ESPG relay click in synchrony with the shutter, thus assuring that the ESPG is switching voltage.

To use the ramp, set the shutter period first and start it going. Watch the ramp output on a scope and adjust the slope until the ramp resets at the proper voltage. For example, if the ADC needs a signal of from 0 to 5 V, adjust the ramp slope so that when it resets the voltage has gotten to a little less than 5 volts. If the period is altered, the slope will of course have to be readjusted.

The shutter box specifications follow and the schematic is shown in Figure C-2. The relays are TTL-compatible reed relays, and NC means normally closed while NO means normally open.

Specifications

PULSER INPUT	Square Wave 0-5 V or -5 V to +5 V
	Pulser = Low yields shutter closed

DELAY	0-10 msec, or 0-1 sec, or off (30 nsec) Front panel switch for range 10-Turn pot reads delay directly (±5%)
RAMP	0 to ±12 V Slope coarse adjust by switch on back Fine slope adjust via 10-turn screwdriver pot Approximate speeds: Fast - 0.036 sec/volt to 0.63 sec/volt Slow - 0.36 sec/volt to 6.3 sec/volt
FAILSAFE	High = Enable Low = Disable
(ANTI)COINC	5 V (0 V) When shutter is closed and delay is over 0 V (5 V) When shutter is open

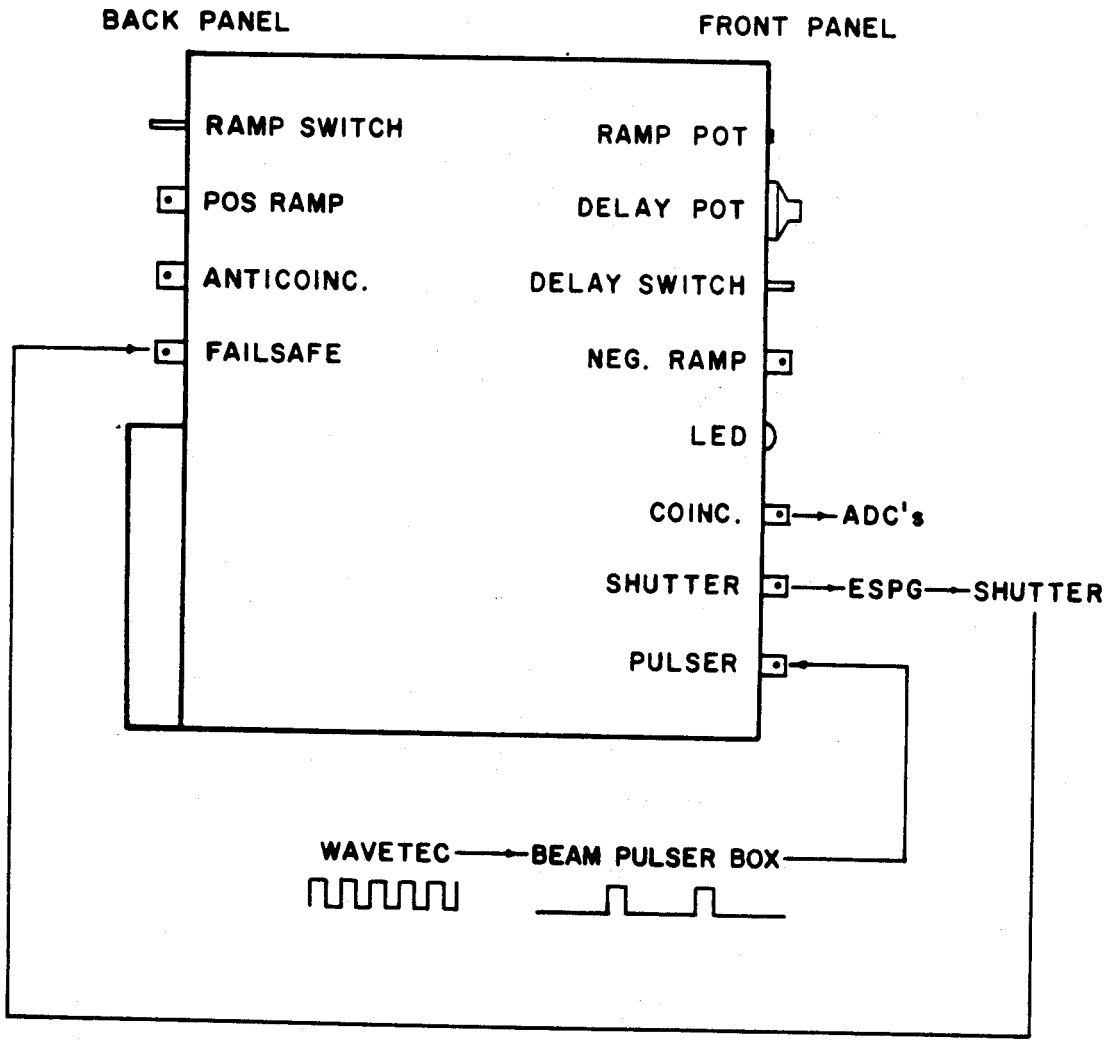

Figure C-1. Overall view of shutter-box functions.

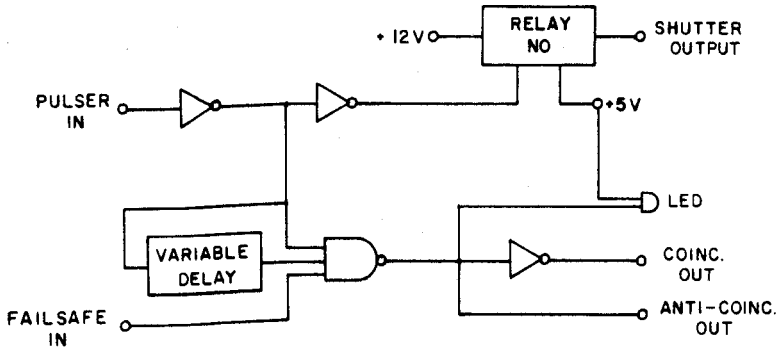

LOGIC

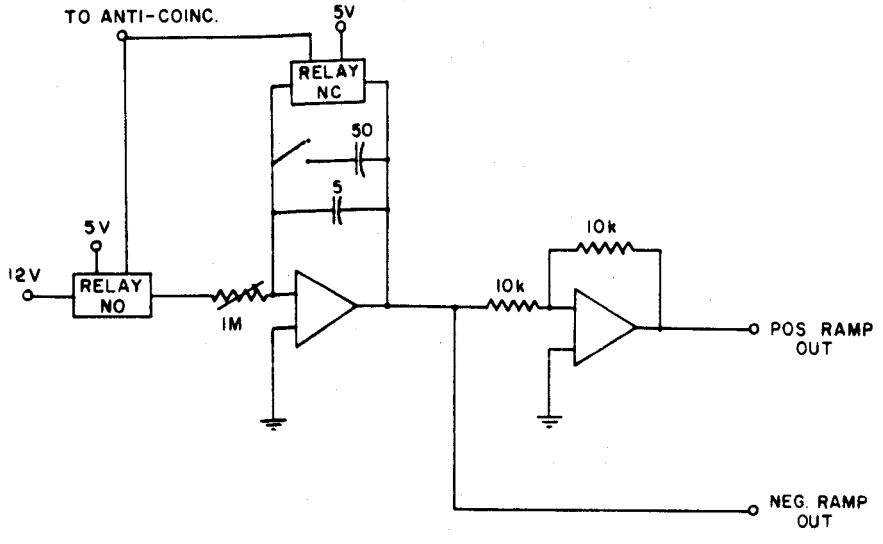

RAMP

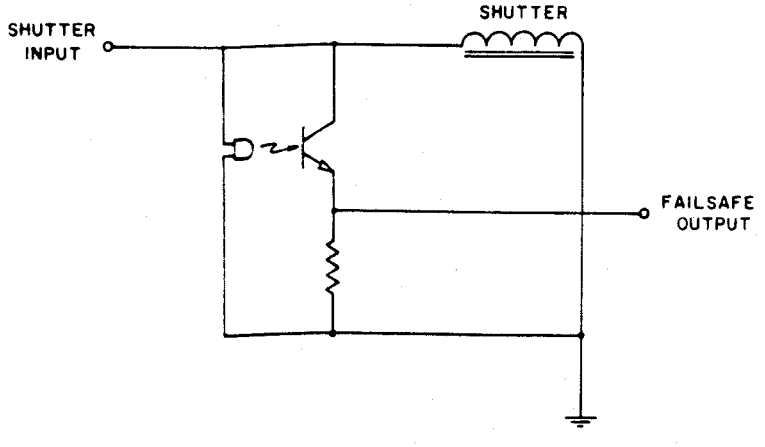

Figure C-2. Schematics of the shutter and the shutter box.

APPENDIX D

THE PRECISION DIGITAL DELAY

Description

The PDD is model 7030 manufactured by Berkeley Nucleonics Corporation. A very complete manual from the manufacturer exists (Be73), so not much will be said here except for a few points which may be overlooked if not mentioned.

Bin Power

The PDD requires ±6 V for operation, whereas most NIM modules do not. Even though most ORTEC bins say ±6 V on them, they were purchased without the ±6 V option. Therefore the PDD can only be used in the specially modified bin next to SIEGFRIED. The -6 V requires a rather large current capability (2 A), so a special power supply was added which has separate +6 V and -6 V power supplies. The schematic of this power supply is shown in Figure D-1. Note that even though the transistor and regulators are heat-sinked, they run a little warm on hot days. A fan was added to help them run cool. Even though the bins in the lab do not have the ±6 V power supply, they do have the wiring bus, so the output of the ±6 V power supply connects to the bus, meaning that all locations in the modified bin are suitable for the PDD.

100-MHz Oscillator

The PDD was designed to divide the 100-MHz signal by 100 and deliver the resulting 1-MHz signal to the "gate out" output upon

grounding a wire internally. A switch was added on the back panel so that this can be done without opening the box. When this option is selected, the box no longer works as a delay, it is just an oscillator. Since the oscillator is very stable (±10 ppm/°C) and contained in an oven, it can be used as a very stable time base for other experiments. This option was used when measuring the mirror half-lives. This option is also used to check the frequency against a standard. There is a coarse frequency adjust (CFA) and a fine adjust (FFA). The CFA is inside the oven and used to be accessible only by dismantling the oven. A small hole was drilled in the oven so that the CFA can be accessed through the top of the box without opening the box. The screw must be carefully located by feel so as not to break any of the small wires of the inductor. This is done with a small screwdriver with a 3-mm × 50-mm shaft. The FFA is also accessible from the top but requires a 3-mm × 200-mm bladed screwdriver.

It has been noticed that the oscillator sometimes starts up at the wrong speed when the power has been interrupted. When this happens the speed is really wrong (≈7.5 MHz instead of 10 MHz). It is therefore suggested that before every run the 1 MHz signal should be switched to the "gate out" output and viewed on a scope to see if it is close to 1 MHz. If so, it is all right. If not, the difference is readily noticeable and the remedy is to turn on and off the bin power or remove and insert the PDD until it resumes proper oscillation. The cause of this behavior is unknown!

Decade Divider

To make the 1 MHz square wave more suitable for other experiments, a simple multi-decade divider was made to divide the 1 MHz by 10^1, 10^2, 10^3, or 10^4. This is simply integrated-circuit dividers powered from the bin supply. The NIM box which contains the dividers also has a LEMO connector with +12 V on it to power the CEMA's emitter-follower. The circuit for this is shown in Figure D-2.

TAC Calibration

To calibrate the TAC, put a pulser into the PDD; start the TAC with the initial pulse; stop the TAC with the delayed pulse. Record (in the ADC) the TAC pulses obtained with several settings of the delay dial. The resulting peaks will be separated by the difference in the delays which were used. This gives a good indication of the presence of or lack of ground loops. If no loops, these peaks will be about 2 or 3 channels wide (FWHM) in a 4096-channel spectrum. If ground loops are present these easily become 10 channels wide or more.

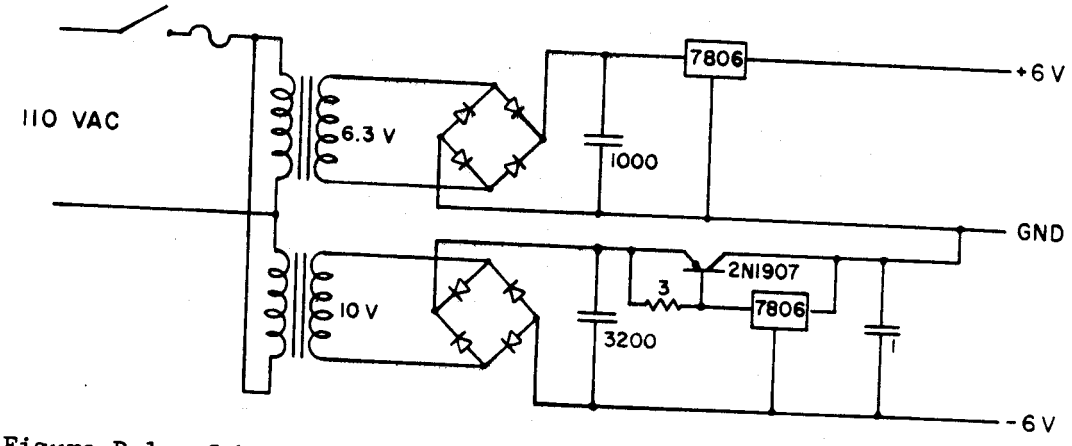

Figure D-1. Schematic of the ±6-V power supply for the PDD.

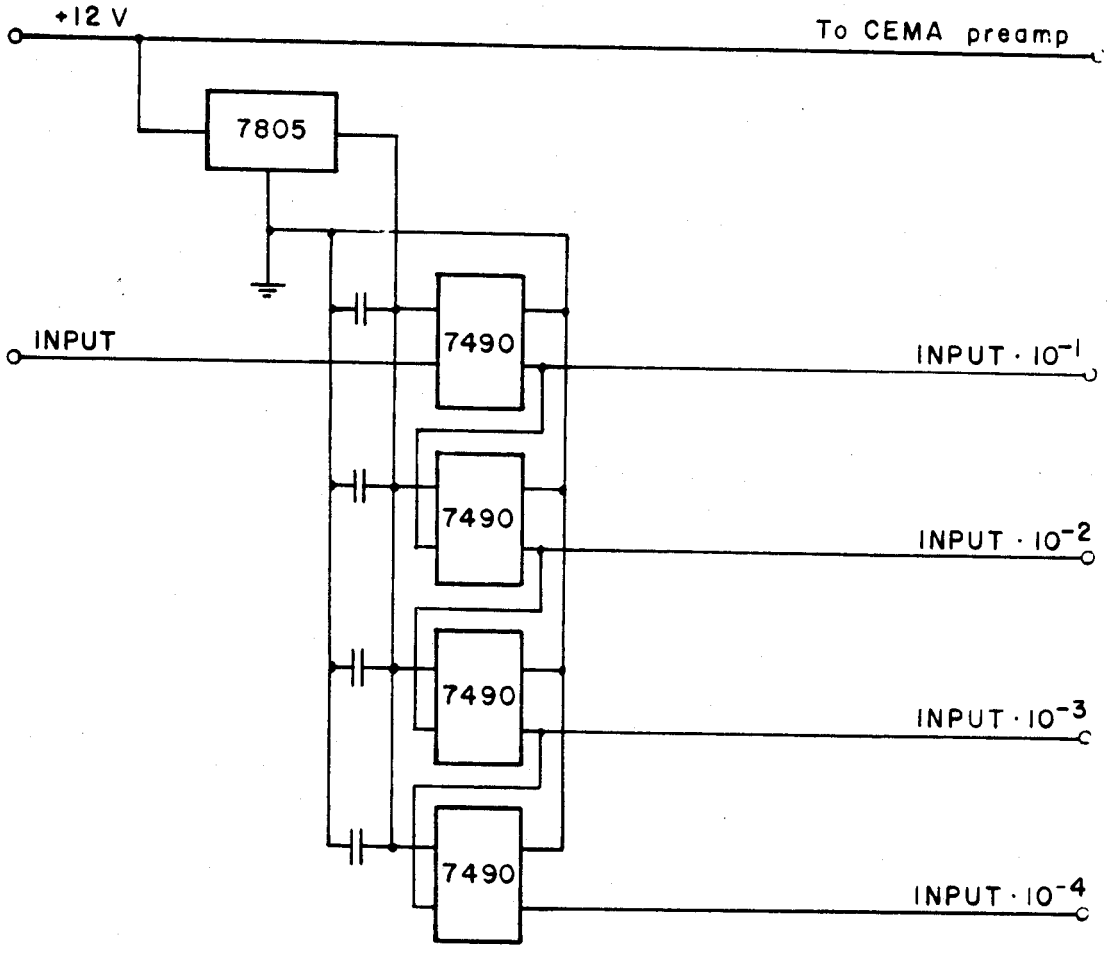

Figure D-2. Schematic of the decade dividers for the PDD oscillator.

APPENDIX E

THE SPELLMAN 30-kV SUPPLY

Description

This supply provides the accelerating voltage (HV) to the collector in SIEGFRIED. It is supposed to have ripple of 10 ppm and stability of 50 ppm/8 hr. Its power requirement is 28 VDC ± 10% and it draws about 1 amp. The output voltage is adjustable from 0 V to 30 kV by a programming voltage of 0 to 6.2 volts. There is an internal 6.2 volt source so only a pot is needed to set the voltage. There is a voltage monitor to observe if the voltage is really present, and there is a current monitor to allow one to watch for sparks of corona discharge.

Although the manufacturer states the supply to be short-circuit proof, spark proof, etc., we have had problems of its Op-amps being destroyed when a large spark occurs. A series resistor was added to help alleviate this problem. If an Op-amp blows, the usual symptoms are no readings on the monitors when the voltage pot is increased. The Op-amp which usually blows is labeled U2 on the circuit board.

The manufacturer has also been very reluctant to give us schematics and technical assistance. If the supply fails to work, and replacing Op-amps does not fix it, it will probably have to be sent back to the manufacturer.

Operation Notes

The proper hookup is shown in Figure E-1. The voltage monitor is 0-100 μA = 0-30 kV, so it is 0.3 kV/μA. The pot is 10 turns from 0-30 kV, so one rotation of the dial is 3 kV. The knob has a calibrated dial on it, and this can be used to set the voltage accurate to about 2 or 3%. The current monitor measures the current drawn, but there is a feedback current for regulation purposes. Therefore the meter reads current even when the load is drawing no current. The feedback current is 3 μA per kilovolt, so at 30 kV the meter should read 90 μA. If it reads greater than this, there is corona discharge, and if sparks occur they are readily apparent.

At this point it may be wise to interject a word of caution about high voltages. The 30-kV supply is quite capable of killing you, as are most of the electronics associated with SIEGFRIED. Always use caution when hooking up and poking around the SIEGFRIED electronics, but use extreme care with the 30-kV supply, because this voltage is high enough to spark over small distances and has been observed to corona discharge over 2-3 cm. It can also breakdown insulation which one would normally consider adequate for voltages usually encountered with the other electronics.

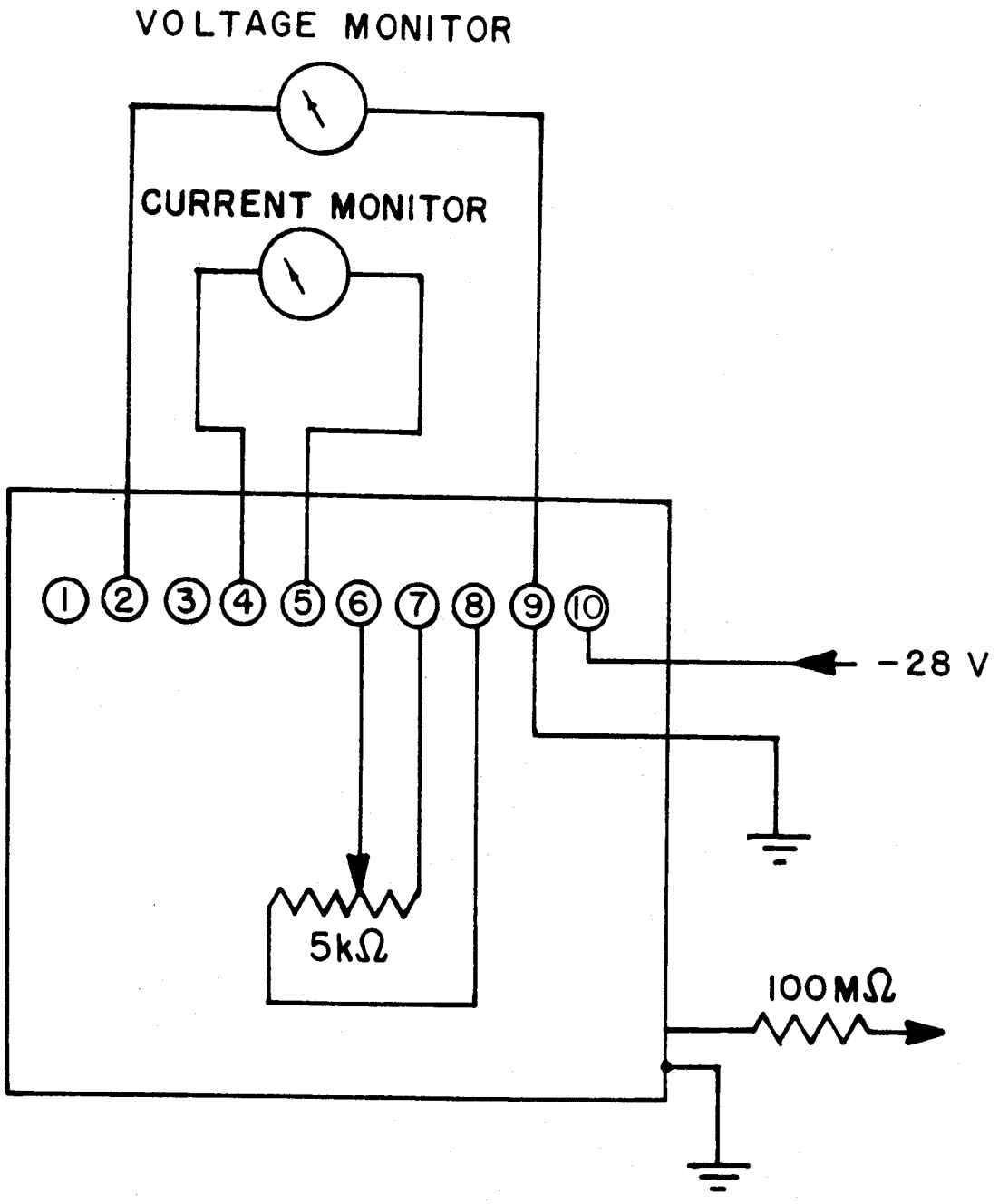

Figure E-1. Schematic of the control circuit for the Spellman supply.

APPENDIX F

THE ESPG SUPPLY

Description

The ESPG supply is a simple voltage doubler circuit which works off the AC line (there is an isolation transformer). The capacitor is charged to the peak voltage (≈350 V) because no current is drawn by the ESPG. The isolation transformer permits the ground to be determined by a voltage divider so that the output may be either +240 V or -110 V with respect to SIEGFRIED's ground.

The output of the shutter box drives a relay which sends the minus or positive voltage to the ESPG depending on the shutter position. There are two shutter inputs hooked in parallel. This prevents the necessity of using a tee connector to route the shutter box output to both the ESPG supply and the shutter.

Higher Voltage Option

If desired, the voltages can be changed by varying the divider resistors (but the sum must still be 350 V). It would also be easy to change to a voltage tripler circuit if higher overall voltages were desired.

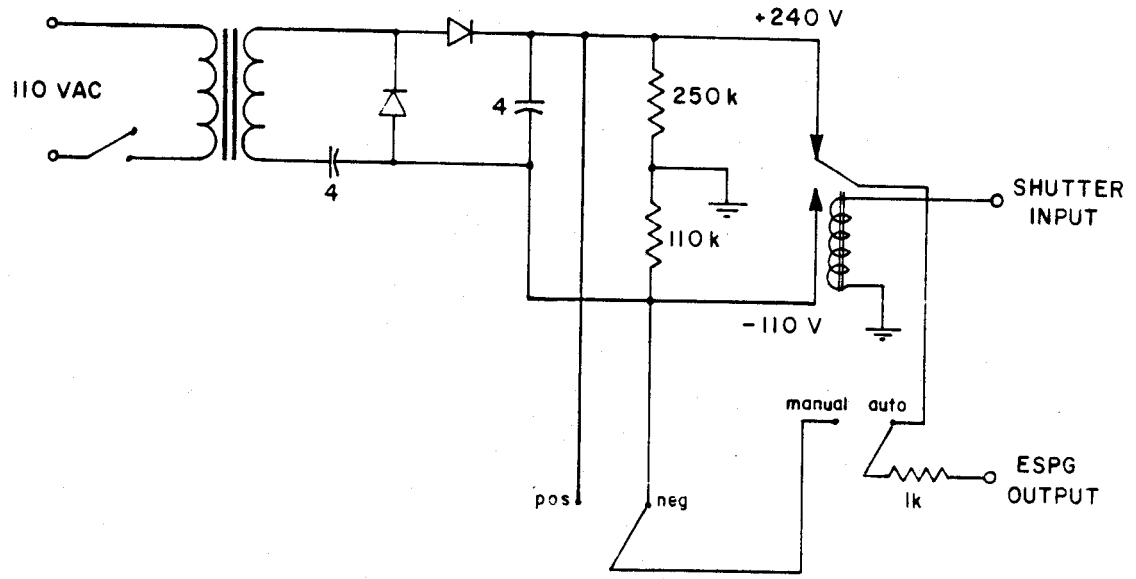

Figure F-1. Schematic of the ESPG dual power supply.

APPENDIX G

TARGET-ARGET

Description

Target-arget (TGT) is a remotely controlled multiple target holder for use with the He-jet. It can hold up to five targets on one slide, and several slides are available. The user can thus choose any of five targets without entering the He-jet vault, and needs enter only once to quickly insert a new slide of five targets. The slides hold the standard 1-inch round target frames usually used with the He-jet. (The slide holes are 1.000 inch so the target frames must be slightly less than 1 inch. Some of the earlier 1.000-inch frames will therefore not work in TGT.)

Design Notes

The slides are driven by a 3-phase motor which is reversed by switching any two of the 3 phases. The third phase is derived from the normal 110 VAC single phase by a series capacitor. Two resistors protect the motor from overheating. The 3-phase power is applied to the motor by one of two 16-volt relays (one relay for each direction). The relays are driven by a logic circuit which senses where the slide is located. The location is achieved by three microswitches inside TGT which are actuated by notches in the slide. The logic not only lets the user know the slide's position, but also prevents him from running the slide into either end! The logic is "read" at the control panel by

six LED's. The LED's indicate that the slide is in one of the five positions or else somewhere between positions.

The schematics for the TGT electronics are given in four parts in Figures G-1 and G-2. All electronics except for the control panel are in one box which is placed inside the vault with TGT. The electronics box is connected to TGT and the control panel with 9-pin connectors. The pin functions appear in Table G-1.

Operating Instructions

Install targets in the slide with the idea that the beam will come from behind the slide (the front side is the side in which the target frames are placed).

Remove the lid from TGT. If a slide is already in place, remove it by holding the switch attached to TGT. (This switch moves the slide only in the out direction and overrides all logic.) Insert the new slide (a locating screw must fit in a groove). When it engages the gear, gently continue pushing until the top of the slide is flush with the top of TGT. It should have some resistance but not much. If it does not coast a little when released, it may be too tight. This is the "load" position. Replace the top. Leave the vault and go to the control panel. The "moving" light will be on. If there are no blank locations in the frame, you may wish to get the cyclotron beam ready before putting the slide into final position. Once the slide has been run in to the first target, it cannot be removed except by going into the vault and using the switch attached to TGT. When ready for a target, push the control panel "in" button. Wait for about 10 sec and the

"#1" light should come on, indicating the first target is in place. The logic is now in control and the slide cannot be moved "out" past #1 and cannot be moved "in" past #5. To switch targets, push and hold the "in" or "out" button until the "moving" light comes on. Release the button and wait. The slide should move to a new position in 5-10 seconds. The "moving" light should then extinguish and a new target-number light should come on. If not, the slide may have stopped, and you need to push the button again.

The device should be foolproof and unjammable. The "in" button overrides the "out" if both are pushed. If the out button is pushed when the slide is in the "load" position, the slide will hit the lid and stall the motor. The resistors protect the motor from overheating, and the remedy is to push the "in" button.

The only fault is that some slides have slightly incorrect notches, which means that the slide may be in a different position than indicated. This is easily recognized by watching the light sequence. Because of this, the logic may occasionally think the slide is at an "end" position when it is not, making motion in that direction impossible. If this happens, simply back the slide up and try again.

Table G-1

TGT Pin Functions

Pin #	Function (logic to CP)	Function (logic to TGT)
1	$\overline{6}$ to lamp 1	NC
2	$\overline{5}$ to lamp 2	+16 V
3	$\overline{2}$ to lamp 3	Switch A_0
4	$\overline{4}$ to lamp 4	Switch A_1
5	$\overline{1}$ to lamp 5	Switch A_2
6	$\overline{7}$ to moving lamp	
7	"in" movement switch	motor drive
8	"out" movement switch	
9	+5 V	+5 V

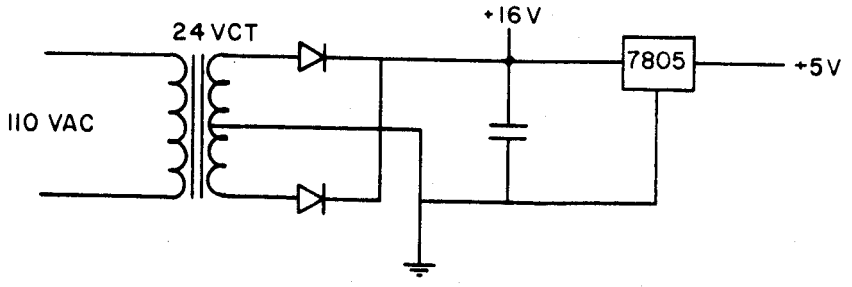

DC POWER SUPPLY

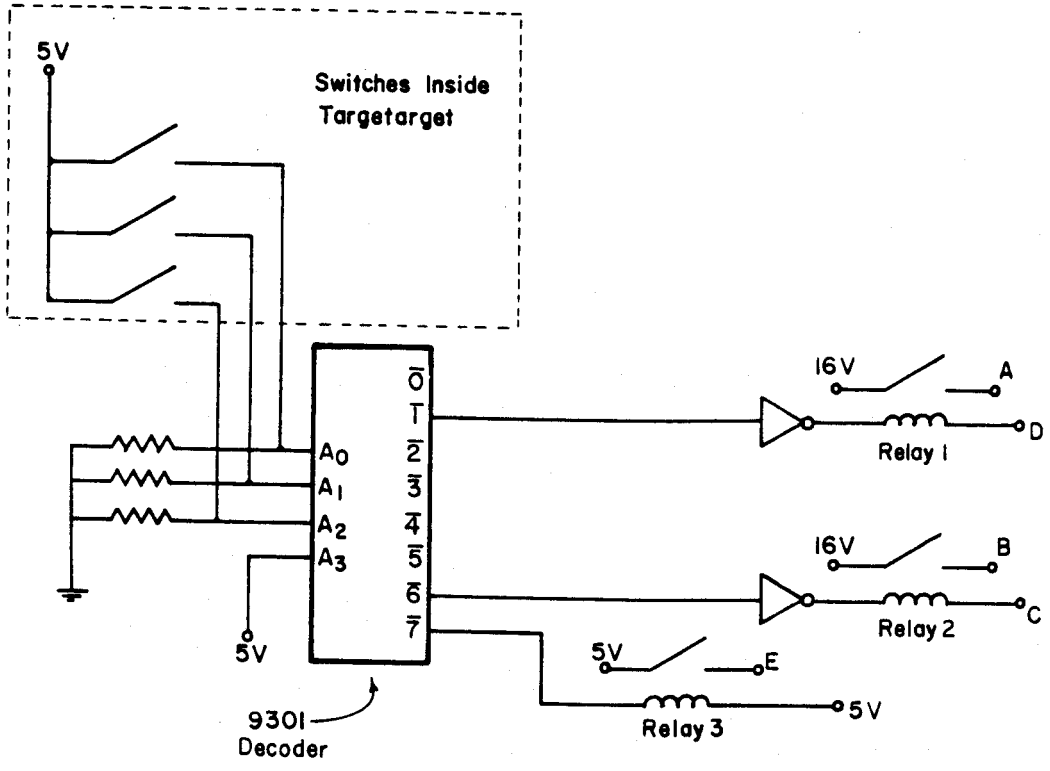

LOGIC SCHEME

Figure G-1. Power supply and logic schematics for TGT.

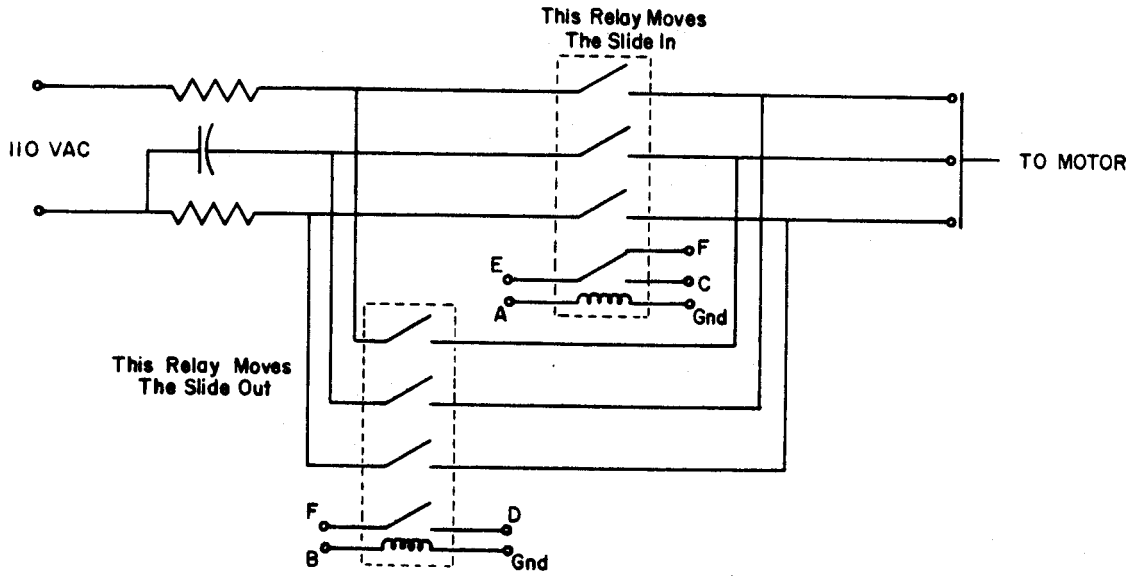

MOTOR RELAYS

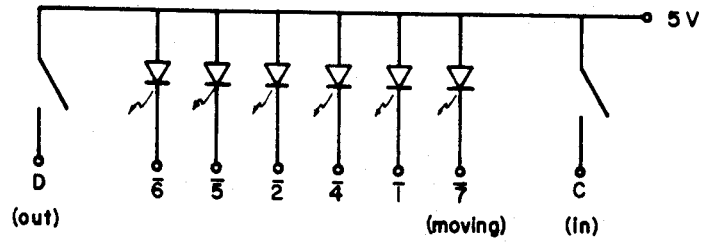

CONTROL PANEL

Figure G-2. Motor-relay and control-panel schematics for TGT.

APPENDIX H

PHOTOGRAPHS

This section is included to give those who have not seen SIEGFRIED an idea of what it looks like. It also is included to show those who have seen SIEGFRIED what some of the internal parts are like.

Figure H-1 was taken from several feet above SIEGFRIED to show the general layout of the parts in which the measurements are made. The capillary can be seen entering the skimmer box next to the knob which adjusts the closeness of the capillary to the skimmer. The port over the skimmer is removed, but the details of the skimmer are difficult to discern. The top of the TOF chamber has been removed to enable one to see the collector and the detector ports. The white ring at the beginning of the flight tube is boron nitride to insulate the collector from the rest of the tube. As can be seen, the collector is very close to the port which contains the plastic scintillator (about 1.6 mm), and sparks sometimes occur between the two when the HV is greater than about 20 kV. With the flight tube shown, the flight length is 1.1 m.

Figure H-2 shows the front view of SIEGFRIED. The black steel frame holds the vacuum chambers and the diffusion pumps. The forepumps are contained on a separate frame. The control panel for the vacuum system can be seen mounted on the main frame. When the forepumps are disconnected (standard 3-inch flanges), and the electricity, water, and air lines are disconnected, the whole frame can be lifted and moved to another location, e.g., another laboratory.

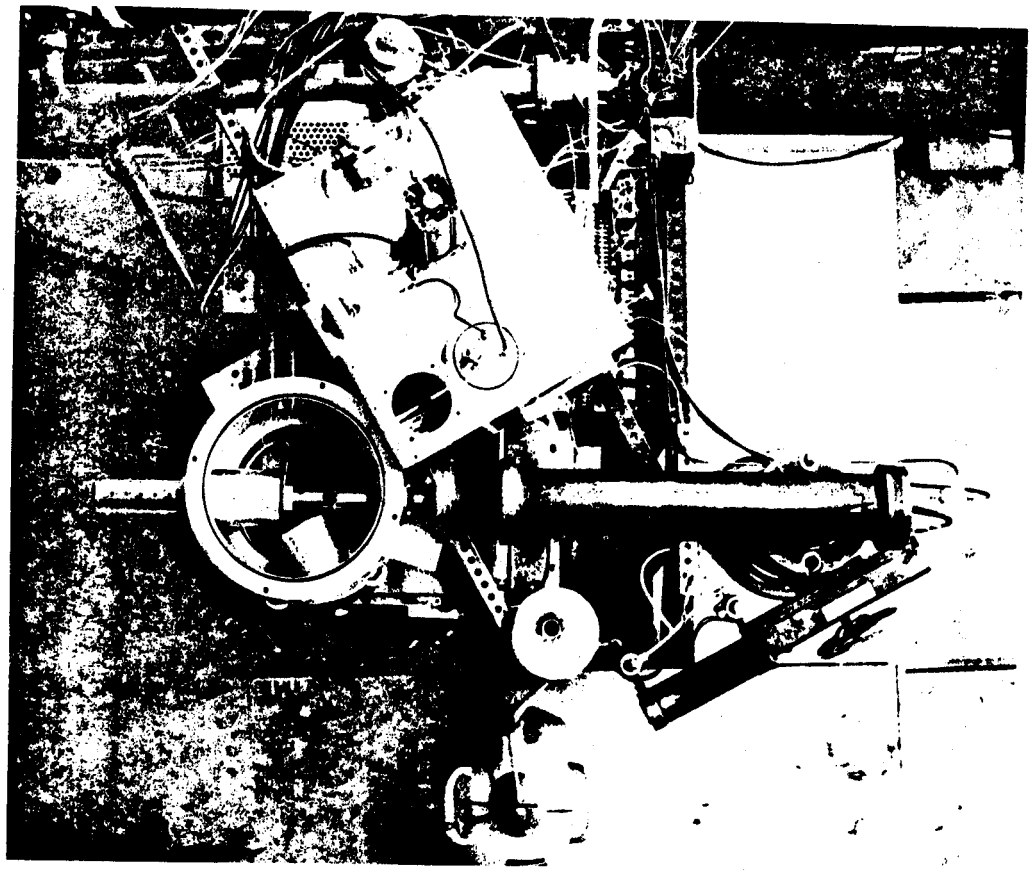

Figure H-1. Overhead view of SIEGFRIED. This photograph is oriented the same as the diagram in Figure 2-1.

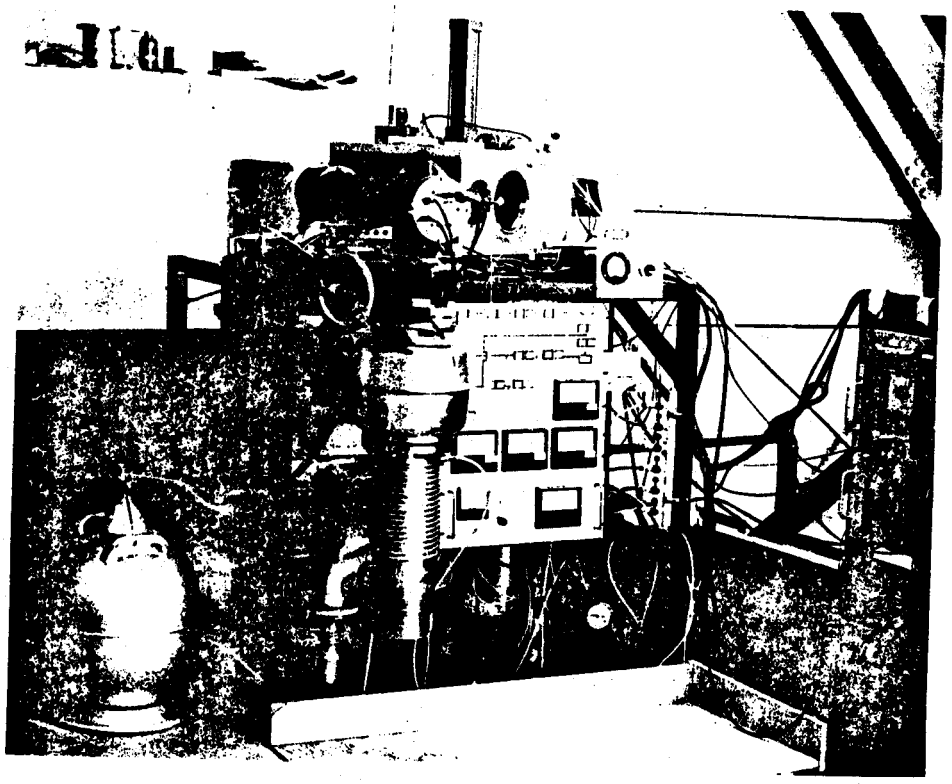

Figure H-2. Front view of SIEGFRIED. The wooden platform is raised about 1 m above the floor to allow easy access to the vacuum chambers. The fore-pumps are beneath the floor.

The Edwards 18B4 booster pump (Edwards High Vacuum Inc., Grand Island, New York) is impressive both in looks and performance. The steel frame was built around the pump and effectively hides it from view. Therefore, Figure H-3 is included to show the pump before it was surrounded by SIEGFRIED.

The CEMA needs no special storage when SIEGFRIED is up to air, so it is rarely removed from the flight tube. It is shown in Figure H-4 attached to its flange. The flange is 15 cm in diameter.

Removing the CEMA uncovers the ESPG mount. This is shown in Figure H-5. The support at the start of the flight path is similar except it is external to the flight tube instead of internal. It can be seen in Figure H-1. The starting end is held by a loop in the wire which goes around monofilament fishing line stretched across the plexiglas ring. The end shown in Figure H-5 is soldered to the support wire which also serves as the power lead.

Since the prototype shutter worked so well that it was never replaced with a fancier design, it is somewhat fragile and is rarely removed. It is shown in Figure H-6. Its full travel is about 4 or 5 mm which is quite adequate. The failsafe arrangement can be seen with the shutter in the down, i.e., skimmer open, position.

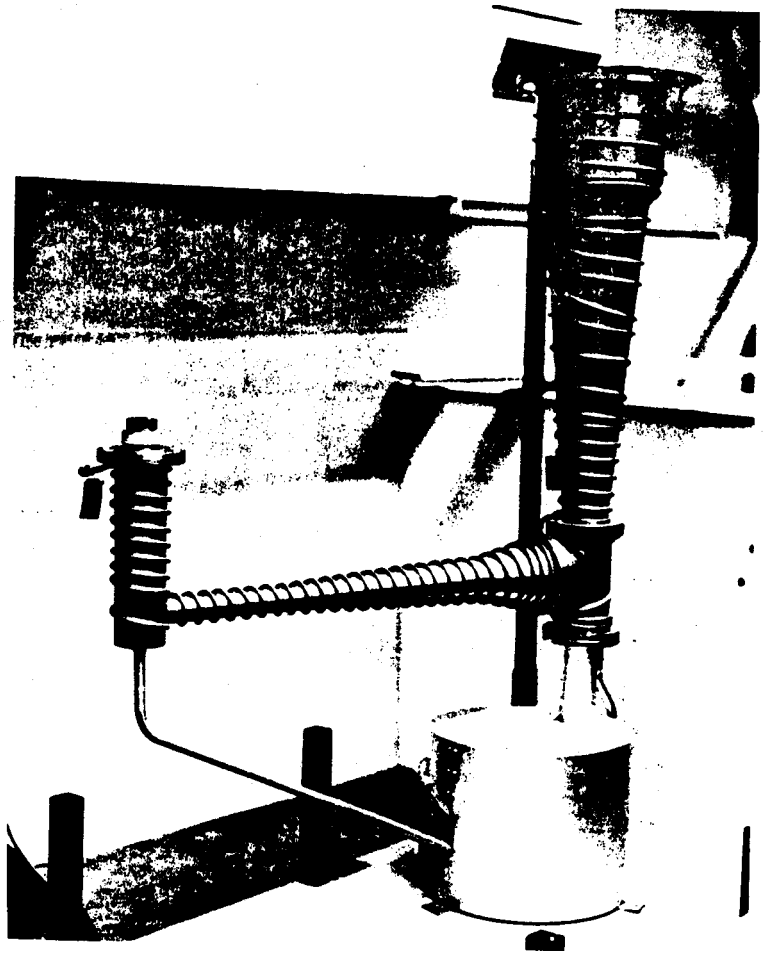

Figure B-3. The Edwards 18B4 booster pump. The pump is nearly 2 m tall and the intake is about 40 cm in diameter. The vertical part contains the diffusion stages and the horizontal part contains the ejector stage.

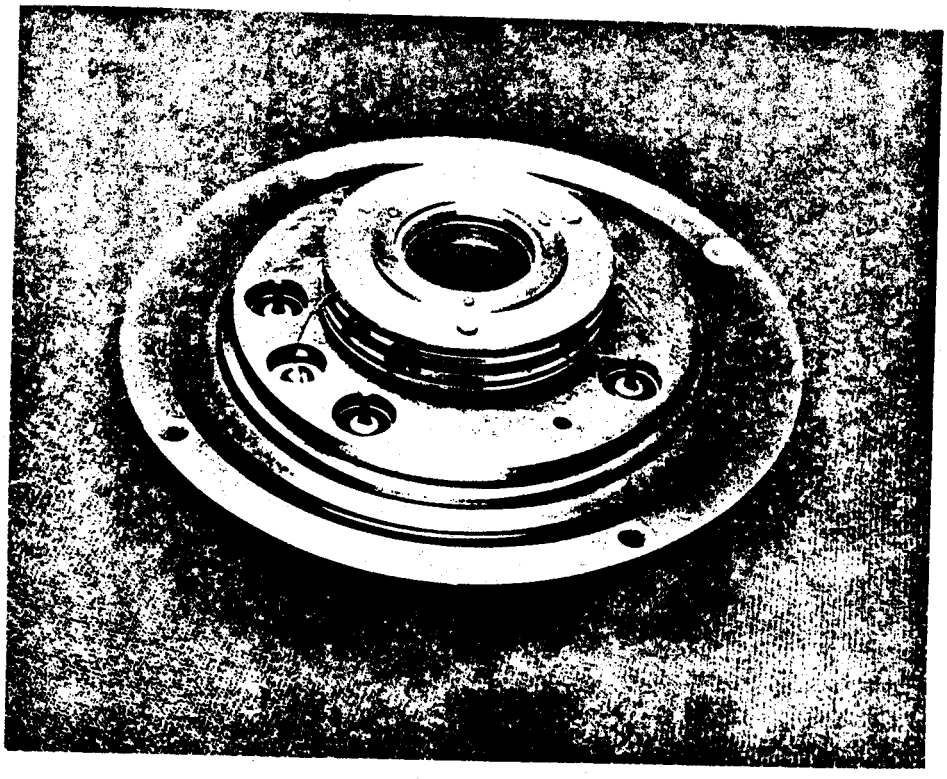

Figure H-4. The CEMA mounted on its flange and ready to be bolted onto the flight tube.

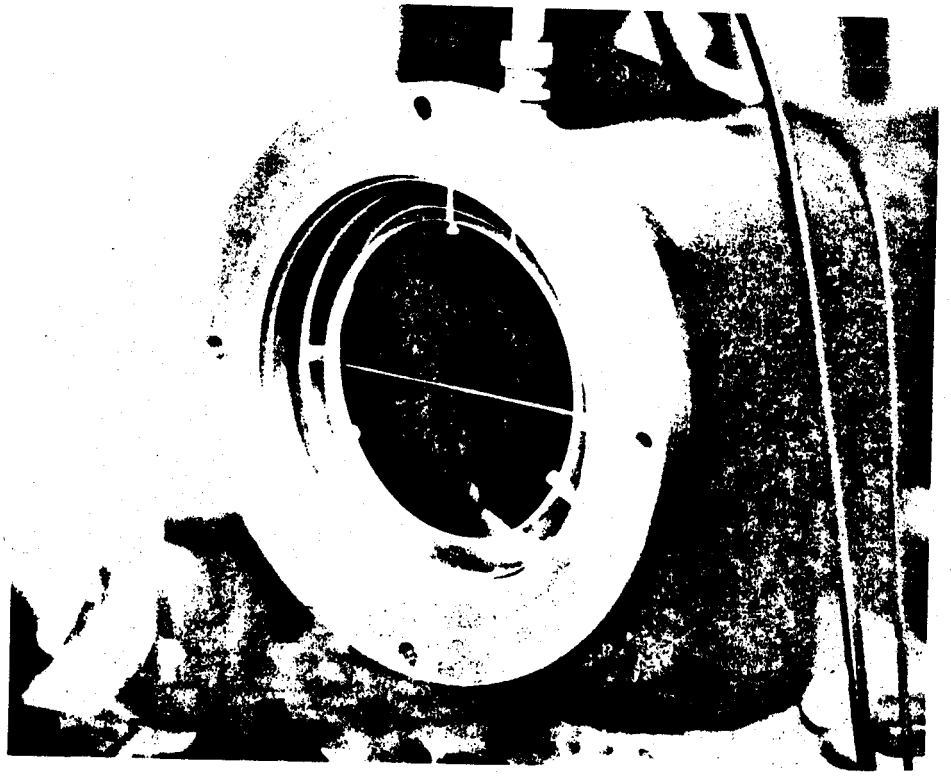

Figure H-5. The end of the flight tube showing the plexiglas ring which holds the ESPG. The ESPG wire is very thin, but it can just be seen as it leaves the support wire.

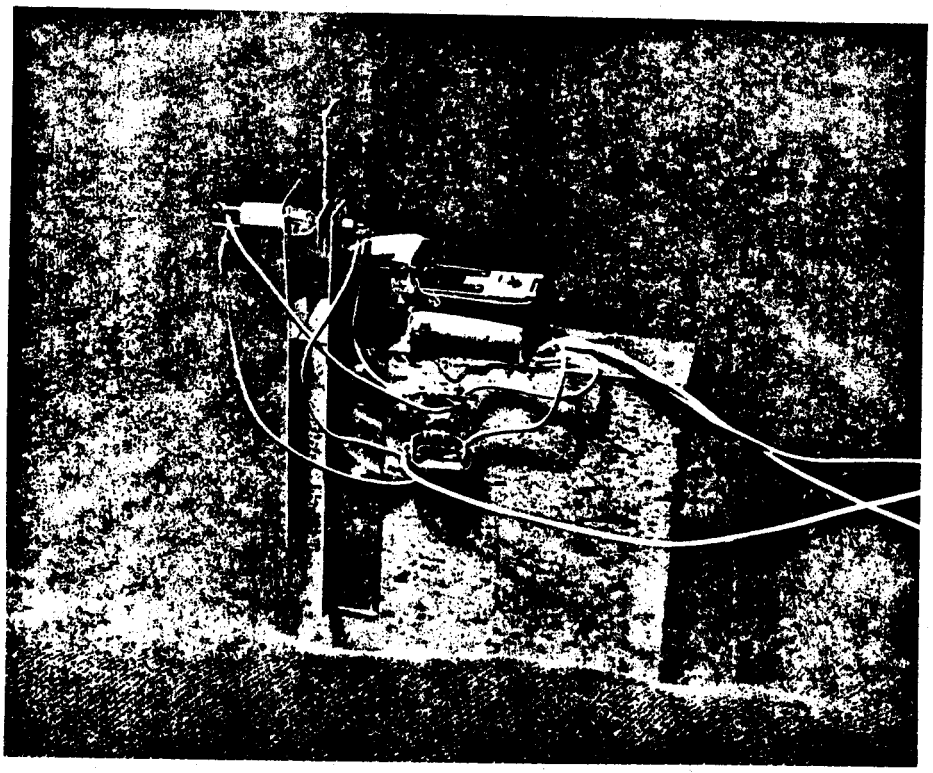

Figure H-6. The shutter and failsafe mechanism.

BIBLIOGRAPHY

BIBLIOGRAPHY

(Be73) _____, Programmable Digital Delay Generator Model 7030, Berkeley Nucleonics Corp., Berkeley, California (1973).

(Bl73) M. Blann and F. Plasil, ALICE: A Nuclear Evaporation Code, U.S.A.E.C. Report No. COO-3494-10 (1973).

(Dy71) J. L. Dye and V. A. Nicely, J. Chem. Ed. 48, 443 (1971).

(Gr75) M. I. Green, P. F. Kenealy, and G. B. Beard, Nucl. Instr. Meth. 125, 1 (1975).

(Ha74) J. C. Hardy, H. R. Andrews, J. S. Geiger, R. L. Graham, J. A. MacDonald, and H. Schmeing, Phys. Rev. Letters 33, 1647 (1974).

(Ju71) H. Jungelas, R. D. Macfarlane, and Y. Fares, Radiochim. Acta. 16, 141 (1971).

(Ko74) K. L. Kosanke, Wm. C. McHarris, R. A. Warner, and W. H. Kelly, Nucl. Instr. Meth. 115, 151 (1974).

(Ko73) K. L. Kosanke, Ph.D. Thesis, Michigan State University, COO-1779-76 (1973).

(Ko75) K. L. Kosanke, M. D. Edmiston, R. A. Warner, Wm. C. McHarris, M. F. Slaughter, and W. H. Kelly, Nucl. Instr. Meth. 125, 253 (1975).

(Le67) C. M. Lederer, J. M. Hollander, I. Perlman, *Table of Isotopes*, New York: John Wiley and Sons, Inc. (1967).

(Ma73) R. D. Macfarlane and Wm. C. McHarris, *Nuclear Reactions and Spectroscopy*, Ed. J. Cerny, New York: Academic Press (1973), Chap. II.C.

(Ma74) R. D. Macfarlane, D. F. Torgerson, Y. Fares, and C. A. Hassell, Nucl. Instr. Meth. 116, 381 (1974).

(Mu74) D. Mueller, E. Kashy, W. Benenson, and H. Nann, Phys. Rev. C 12, 51 (1975).